Post-collisional magmatism and ore-forming systems in the Menderes Massif: new constraints from the Miocene porphyry Mo–Cu Pınarbaşı system, Gediz–Kütahya, Western Turkey

Okan Delibaş[1§], Robert Moritz[2*], Massimo Chiaradia[2], David Selby[3], Alexey Ulianov[4], Mustafa Kemal Revan[5]

[1]: Department of Geological Engineering, Hacettepe University, 06800, Beytepe-Ankara, Turkey

[2]: Department of Earth Sciences, University of Geneva, Rue des Maraîchers 13, 1205 Geneva, Switzerland

[3]: Department of Earth Sciences, Durham University, Durham DH1 3LE, United Kingdom

[4]: Institute of Earth Sciences, University of Lausanne, Géopolis, 1015, Lausanne, Switzerland

[5]: General Directorate of Mineral Research and Exploration (MTA), 06800, Ankara, Turkey

*Corresponding author: Department of Earth Sciences, University of Geneva, Rue des Maraîchers 13, 1205 Geneva, Switzerland. e-mail: robert.moritz@unige.ch

§ Deceased August 23, 2016

Key Words: Post-collisional magmatism, Porphyry type mineralization, Ore-forming systems, Re-Os molybdenite ages, Western Anatolia, Turkey

Abstract

The Pınarbaşı Mo–Cu prospect is hosted within the Pınarbaşı intrusion, which is exposed together with the NW–SE-trending Koyunoba, Eğrigöz, and Baklan plutons along the northeastern border of the Menderes massif. The Pınarbaşı intrusion predominantly comprises monzonite, porphyritic granite, and monzodiorite. All units of the Pınarbaşı intrusion have sharp intrusive contacts with each other. The principal mineralization style at the Pınarbaşı prospect is a porphyry-type Mo–Cu mineralization hosted predominantly by monzonite and porphyritic granite. The porphyry type Mo–Cu mineralization consists mostly of stockwork and NE- and EW-striking sub-vertical quartz veins. Stockwork-type quartz veins hosted by the upper parts of the porphyritic granite within the monzonite, are typically enriched in chalcopyrite, molybdenite, pyrite, and limonite. The late NE- and EW-striking normal faults cut the stockwork vein system and control the quartz–molybdenite–chalcopyrite–sphalerite–fahlore–galena veins, as well as molybdenite–hematite-bearing silicified zones.

Lithogeochemical and whole-rock radiogenic isotope data (Sr, Nd and Pb) of the host rocks, together with Re-Os molybdenite ages (18.3 ± 0.1 Ma – 18.2 ± 0.1 Ma) reveal that the monzonitic and granitic rocks of the Pınarbaşı intrusion were derived from an enriched lithospheric mantle-lower crust during Oligo–Miocene post-collisional magmatism. The lithospheric mantle was metasomatised by fluids and subducted sediments, and the mantle-derived melts interacted with lower crust at 35-40km depth. This mechanism explains the Mo and Cu enrichments of the Pınarbaşı intrusion during back-arc magmatism. We conclude that the melt of the Pınarbaşı intrusion could have rapidly ascended to mid-crustal levels, with only limited crustal

assimilation along major trans-lithospheric faults as a result of thinning of the middle to upper crust during regional extension, and resulted in the development of porphyry-style mineralization during the early Miocene (~18 Ma). The subsequent exhumation history of the Mo–Cu-bearing Pınarbaşı intrusion is attributed to regional-scale uplift, and further exhumation along detachment faults of the associated core complexes during the middle to late Miocene.

1. Introduction

The Aegean Sea region belongs to the Tethys orogenic belt, and it is one of the Cenozoic Mediterranean back-arc basins with the fastest rates of ongoing extension on Earth, resulting in rapid thinning of the continental crust, detachment faulting, exhumation of metamorphic domes, formation of supradetachment sedimentary basins, and abundant post-orogenic magmatism (Bozkurt et al. 1993; Hetzel et al. 1995; Bozkurt and Park 1997; Ring et al. 1999, 2010; Koçyiğit et al. 2000; Doglioni et al. 2002; Whitney and Bozkurt 2002; Bozkurt and Sözbilir 2004; Dilek et al. 2009; Agostini et al. 2010). Ages of metamorphic dome exhumation and post-orogenic magmatism exhibit a younging from north to south in the Aegean Sea region towards the Hellenic trench (Jolivet et al. 2003; Jolivet and Brun 2010). This geodynamic setting also provided a particularly favorable environment for the concentration of a large variety of metal resources in the Earth's crust, as documented by the abundant Cu, Au, and Pb-Zn deposits and prospects associated with the metamorphic domes and/or post-orogenic magmatic provinces of the Aegean Sea region (Oygür 1997; Arikas and Voudouris 1998; Oygür and Erler 2000; Marchev et al. 2005; Yigit, 2009; Márton et al. 2010; Moritz et al. 2010, 2014; Voudouris et al. 2010; van Hinsbergen and Schmid 2012; Kaiser-Rohrmeier et al. 2013; Sánchez et al. 2016; **Fig. 1**).

The Middle to Late Cenozoic Cu-Mo±Au-bearing porphyry systems within different segments of the Tethys metallogenic belt, from the Aegean region through Anatolia to the Lesser Caucasus, are closely associated with the post-collisional evolution of the Tethys metallogenic belt (Konos Cu-Mo, Skouries Cu-Au-Mo, Pagoni Rachi Cu-Mo-Ag-Au in Greece: Voudouris et al. 2010; 2013a, b; Kisladag Au-Mo in Turkey: Sillitoe 2002, Yiğit 2009; Kerman Porphyry Cu-Mo belt in Iran: Aghazadeh et al. 2015; Kadjaran Cu-Mo in Armenia: Moritz et al. 2016, Rezeau et al. 2016). The Oligocene to Miocene, Greek Mo-Re-bearing porphyry systems in the Cenozoic Mediterranean back-arc basin are closely linked to shoshonitic to calc-alkaline magmatism that were produced by sub-continental lithospheric mantle–lower crust interaction within a post-orogenic setting (Kroll et al. 2002; Voudouris et al. 2010, 2013a, b). In particular, the link with the regional tectono-magmatic evolution of Eocene to Oligocene (~38 – 29 Ma) ore deposits/prospects of the oldest and northernmost metamorphic dome province of the Aegean region in the Rhodope Massif in Bulgaria and Greece has been addressed in detail (Arikas and Voudouris 1998; Marchev et al. 2005; Márton et al. 2010; Moritz et al. 2010, 2014; Kaiser-Rohrmeier et al. 2013).

The northern zone of the Menderes Massif in Turkey is well endowed with numerous mineral deposits/prospects and a large variety of commodities (**Fig. 1**), including porphyry-type Mo–Cu–Au, skarn-type Fe and Pb–Zn, base metal and precious metal epithermal deposits/prospects (Gökce and Spiro 1994; Oygür and Erler 2000; Yiğit 2006, 2009; Delibaş et al. 2012a, b Oyman et al. 2013). Some of the deposits and prospects are spatially associated with post-collisional magmatic activity such as the

Ovacık Au-Ag deposit, with grabens at the Kurşunlu and Emirli Au-Ag-Sb-Hg-bearing prospects, and the hanging- and footwalls of post-collisional detachment faults (**Fig. 1**; Yiğit 2006). Nevertheless, the link between post-collisional metallogenic evolution, magmatism and extension remains poorly documented and constrained in the Menderes Massif.

This study addresses the petrogenesis of ore-bearing felsic intrusions and the timing of mineralization during post-orogenic evolution of the Menderes Massif in western Anatolia. In this contribution, we report field observations from the Mo–Cu-Pınarbaşı prospect, Re-Os molybdenite age data from the main mineralization stage, lithogeochemical, and whole-rock radiogenic isotope data (Sr, Nd and Pb) from the associated Oligo-Miocene granitic and monzonitic host rocks. Our aim is to constrain the timing of mineralization, and its genetic link with the ore-associated magmatic rocks and the geodynamic evolution of the Gediz-Pınarbaşı region.

2. Regional Geology

Following final accretion of the Gondwana-derived Sakarya block to the southern Eurasian margin during the Late Cretaceous–Paleocene (Şengör and Yilmaz 1981; Okay and Tüysüz 1999), western Anatolia underwent widespread extension from the Oligo–Miocene to the present. Previous studies have concluded that the complex extensional tectonic evolution has resulted in exhumation of metamorphic core complexes, emplacement of felsic intrusions along shear zones, block faulting and graben formation (Bozkurt et al. 1993; Hetzel et al. 1995; Ring et al. 1999; Koçyiğit et al. 2000). Western Anatolia is segmented into several thrust-bounded metamorphic zones, and includes from north to south: the Tavşanlı zone, the Afyon zone, and the

Menderes Massif (**Fig. 1, inset;** Şengör et al. 1984; Okay et al. 1998; Sherlock 1999; Okay 2008; van Hinsbergen 2010). The oldest units in the region are the Menderes Massif metamorphic rocks, which are tectonically overlain by the Lycian Nappes in the south and the oceanic remnants of the Neo-Tethys in the north (Collins and Robertson 1997; Bozkurt 2004). The northern and northeastern borders of the Menderes Massif are crosscut by Cenozoic diorite, quartz diorite, monzonite, granodiorite and granite. Three main magmatic episodes are recognized: 1) middle to late Eocene, 2) Oligo–Miocene, and 3) middle-late Miocene to recent (Innocenti et al. 2005; Ring and Collins 2005; Hasözbek et al. 2010; Karaoğlu et al. 2010; Altunkaynak et al. 2012a, b). Although their origin has been hotly debated, the Eocene calc-alkaline felsic intrusions (55 – 38 Ma) are generally attributed to subduction-related magmatism, partly sourced by metasomatised lithospheric mantle during convergence and subsequent collision of the Sakarya and Anatolide–Tauride blocks along the Izmir-Ankara subduction zone (IASZ) (Harris et al. 1994; Aldanmaz et al. 2000; Koprubasi and Aldanmaz 2004; Altunkaynak et al. 2012b).

The duration of the second, Oligo–Miocene calc-alkaline to high-K calc-alkaline magmatic cycle is well constrained between ~24.0 and 19.5 Ma with U-Pb zircon ages from granite (Ring and Collins 2005; Hasözbek et al. 2010; Altunkaynak et al. 2012a) and $^{40}Ar/^{39}Ar$ (hornblende, biotite) ages record cooling ages of the Oligo-Miocene granites that range between ~25 and 18 Ma, indicating fast cooling (Isik et al. 2004; Aydoğan et al., 2008; Altunkaynak et al. 2012a). However, the origin of the Oligo-Miocene magmatism remains open to question. Several models have been proposed, including: 1) back-arc magmatism during southward roll-back and retreat, as the African and Eurasian plates were converging, resulting in partial melting of the

lower crust during asthenospheric upwelling (Fytikas et al. 1984; Delaloye and Bingöl 2000; Pe-Piper and Piper 2001, 2007; Jolivet and Brun 2010; Ring et al. 2010; Jolivet et al. 2015); 2) decompressional melting related to orogenic collapse of an overthickened crust, at the late Oligocene-early Miocene transition (Seyitoglu et al. 1992; Seyitoglu 1997); and 3) post-collisional magmatism sourced by melting of lithospheric mantle metasomatised during the preceding subduction stage, and induced by asthenospheric upwelling. The latter is attributed to the Sakarya-Taurides-Anatolides continent collision in the north and the subsequent extensional stage related to subduction of the Aegean slab along the Hellenic arc (Aldanmaz et al. 2000; Altunkaynak and Dilek 2006; Dilek et al. 2009). The Oligo–Miocene magmatism accompanied a two-stage regional extension of western Anatolia, starting with late Oligocene to early Miocene detachment faulting, such as the Simav fault zone (**Fig. 1**), and late Oligocene to middle Miocene core complex exhumation in the Menderes Massif, followed by graben formation with high-angle normal faulting from middle to late Miocene (Pourteau et al. 2010; **Fig. 1**). The general agreement is that the local granitic intrusions, named Eğrigöz, Alaçam and Koyunoba (**Fig. 1**), are syn-tectonic, and that they intruded Paleozoic basement along the footwall of the Simav detachment fault zone during early extension and metamorphic core exhumation in the early Miocene (Isik et al. 2004; Dilek et al. 2009; Erkül 2010; Erkül et al. 2013).

The last pulse of Cenozoic magmatism in the region consists of intraplate shoshonitic to mildly alkaline and following OIB-type magmatism, during thinning of the Aegean–Anatolian lithosphere in response to extension since the middle-late Miocene (Doglioni et al. 2002; Innocenti et al. 2005; Agostini et al. 2007, 2010; Karaoğlu et al.

2010; Ersoy and Palmer 2013). The middle-late Miocene to early Pliocene pulse of magmatism is mainly mildly alkaline to shoshonitic in nature and it shows a within-plate character (Innocenti et al. 2005; Helvacı et al. 2009). On the other hand, the early Pliocene to Quaternary phase of magmatism comprises sodic and potassic magmatism and it displays clear OIB-type signatures (Alici et al. 2002; Innocenti et al. 2005; Ersoy and Palmer 2013).

3. Geological setting of the Pınarbaşı Mo–Cu prospect

In the Gediz-Pınarbaşı region, the stratigraphic column comprises, from bottom to top, Menderes Massif metamorphic rocks and low-temperature, high-pressure meta-sedimentary units of the Afyon zone, followed by the Triassic–Jurassic Kırıkbudak Formation composed of alternating sandstone, siltstone and limestone units with an estimated thickness of 200 to 750 m, and a Late Triassic to Maastrichtian dolomitized, platform-type limestone unit, known as the Budağan limestone with an estimated thickness of 150 to 600 m (Akdeniz and Konak 1979; Okay et al. 1996; Candan et al. 2005). These stratigraphic units are overthrusted by Cretaceous to Paleocene ophiolitic mélange units, mostly comprising radiolarite, large limestone-marble blocks, tuffite, and peridotite with a thickness of more than 750 m (Akdeniz and Konak 1979). These rocks were intruded by early Miocene felsic rocks and their sub-volcanic equivalents, including the Eğrigöz, Koyunoba, and Pınarbaşı intrusions and the Simav volcanic rocks (**Figs. 1 and 2a-b**). The NW-trending Mo–Cu-bearing, multiphase, calc-alkaline Pınarbaşı intrusion is crosscut by NW- and NS-striking andesitic, dacitic, and aplitic dykes, and NE- and EW-striking Mo–Cu-bearing quartz veins, whereas the limestone and mélange units are crosscut by NW-trending porphyry dikes (Delibaş et al. 2012a, b). The eastern zone of the mapped area is

dominated by Neogene and Quaternary volcano-sedimentary cover sequences (**Fig. 2a**).

The NW-trending active Simav and Kutahya fault zone next to the Pınarbaşı prospect resulted in complex EW-, NW-, and NE-oriented block faulting (Tokay and Doyuran 1979; **Fig. 1, and inset in Fig. 2**). The Pınarbaşı intrusion is exposed on the northwestern shoulder of the Yenidoğmuş–YeniGediz graben, and is controlled by the NE-striking Eskigediz normal fault and the EW- to NW-oriented Şaphane normal fault zone, which are associated with graben formation (Gürboğa et al. 2013; **inset in Fig. 2**). The latter fault zone hosts the Şaphane deposit, which is the largest epithermal alunite deposit of Turkey (Mutlu et al. 2005). Three generations of fault systems have been recognized, including EW- and NW-striking normal faults, NE-trending normal faults, dipping 70–80° to the NW (**Figs. 3a-b**), and late-stage NS-, NW-, and NE-striking strike-slip local fault systems, which are largely developed along the vertical contacts between the intrusion and limestone, and which crosscut the hydrothermal alteration zones as well as earlier faults. The Pınarbaşı intrusion is strongly mylonitized along its contact with the intensely silicified country rock (**Fig. 3c**). This masks the contact between the intrusion and its country rocks, and conceals the late contact metamorphism along the margins of the intrusion (Delibaş et al. 2012a**; Fig. 3c)**. However, 0.5 to 1m-wide skarn zones containing garnet, epidote, pyroxene, calcite, and magnetite are developed along the contacts of the NW-trending porphyritic dykes crosscutting the limestone and the mélange units (**Fig. 3d**).

The Pınarbaşı intrusion primarily comprises monzonite, porphyritic granite, and monzodiorite (Delibaş et al. 2012a, b), which have sharp intrusive contacts with each other (**Fig. 3a**). They contain roughly oval, fine-grained dioritic enclaves, with sharp contacts with their host rocks. The largest intrusive body in the area is a fine- to medium-grained monzonite with a largely equigranular texture. It predominantly contains highly sericitized euhedral to subhedral plagioclase, subhedral K-feldspar, subhedral to euhedral amphibole, biotite, pyroxene, minor quartz, and accessory apatite. Epidote, calcite, chlorite, and sericite are alteration products of the main mineral assemblage. A porphyritic granite cutting the monzonite is exposed in the western part of the area (**Fig. 3e**). The intrusion of the porphyritic granite into the monzonite resulted in the formation of an intrusion breccia (Delibaş et al. 2012a; **Fig. 3f)**. The porphyritic granite is characterized by a more pronounced porphyritic texture, consisting of plagioclase, biotite and K-feldspar phenocrysts within a fine-grained matrix consisting of K-feldspar, plagioclase, biotite, amphibole, and quartz. The monzonite and porphyritic granite are cut by bodies of dark-gray diorite and monzodiorite with an equigranular to porphyritic texture. They have the same mineralogical composition as the dioritic enclaves and generally consist of sericitized plagioclase, amphibole, biotite, pyroxene, and minor quartz.

4. The Pınarbaşı porphyry Mo–Cu-type prospect

The Pınarbaşı Mo–Cu prospect is hosted by the Pınarbaşı intrusion, which is exposed approximately 20 km southeast of the NW-trending active Simav fault zone. The latter fault also hosts small to mid-scale high- and low-sulfidation epithermal and Cu–Pb–Zn vein-type mineralization within the southern sector of the Afyon zone (Oygür and Erler 2000; **Fig 1**). Based on drill hole data, the Cu and Mo contents of

the prospect vary between 374 and 34,800 ppm, and between 106 and 2,200 ppm, respectively (Delibaş et al. 2012b).

The principal mineralization style at the Pınarbaşı prospect is a porphyry Mo–Cu type mineralization hosted predominantly by monzonite and porphyritic granite. Field, mineralogical, and lithogeochemical studies have also revealed the presence of Pb and Zn enrichments up to 6.7 wt. % and 7700 ppm, respectively, within the Budağan limestone (Oygür and Erler 2000; Delibaş et al. 2012a,b). In addition, Sb, Ag and Au grades up to 1210 ppm, 12 ppm, and 1320 ppb, respectively, have been reported within the silicified zones along the NW-striking, normal and strike-slip faults cutting the limestone blocks of the ophiolitic mélange units and Sb, Ag, Au and Pb-rich silicified zones within limestone blocks mainly show lattice textures (e.g., primary bladed calcite, ghost bladed quartz, lattice bladed quartz), indicating a low-sulfidation epithermal mineralization at relatively shallow depths (Delibaş et al. 2012b).

The porphyry-type Mo–Cu mineralization consists mostly of stockwork and NE- and EW-striking sub-vertical quartz veins (**Figs. 4a-b**). Stockwork-type quartz veins within the upper parts of the porphyritic granite typically contain chalcopyrite, molybdenite, pyrite, and limonite. Late NE- and EW-striking normal faults, crosscutting the stockwork mineralization, host quartz–molybdenite–chalcopyrite–sphalerite–sulfosalts–galena veins and molybdenite–hematite-bearing silicified zones (**Figs. 4c-e)**. Potassic, sericitic, and argillic alterations are associated with the Mo–Cu mineralization (Oygür and Erler 2000; Delibaş et al. 2012a, b). The local potassic alteration zone within porphyritic granite of the Pınarbaşı intrusion is characterized by small magnetite, biotite, and 1–5 cm thick K-feldspar veins (**Figs. 5a-b**). Sericitic

alteration is developed along the NE- and EW-striking ore-controlling faults, where advanced argillic alteration is less intense, and it is dominated by sericite–muscovite, pyrite, hematite, and small quartz veinlets (**Figs. 4b-c and 5c-d**). Sericitic alteration grades locally into intense silicification, which contains small molybdenite-bearing stockwork quartz veinlets. The intensity of silicification decreases away from the main fault zones. Creamy to white advanced argillic alteration predominates at Pınarbaşı and overprints the sericitic and potassic alterations. It primarily comprises pyrophyllite, tabular alunite, fluorite, kaolinite, and illite (**Figs. 5e-f**). Jarosite, smectite, and Fe-oxides along the late-stage normal and strike-slip faults are interpreted as supergene alteration. Based on field observations, mineralization styles, and alteration types, the Pınarbaşı prospect is interpreted as a porphyry-style Mo–Cu mineralization, telescoped by low-sulfidation epithermal Sb ± Ag ± Au ± Pb mineralization and an intense advanced argillic alteration zone. Late supergene alteration along younger fault zones overprints the earlier associations (Oygür and Erler 2000; Delibaş et al. 2012a).

5. Results

Seventeen fresh rock samples from the Pınarbaşı granitoid were selected for whole-rock lithogeochemistry analysis. Samples showing hydrothermal alteration effects were removed and we used plutonic and subvolcanic rock samples revealing loss of ignition (LOI) below 2.0 wt. % for petrologic interpretations to avoid potential hydrothermal alteration effects. Twelve whole-rock powder samples were analyzed for radiogenic isotopic compositions (Sr, Nd, Pb). Radiogenic isotope analyses were conducted at the University of Geneva, Switzerland. We also report two new Re-Os molybdenite ages from the main mineralization stage. The ^{187}Re and ^{187}Os

concentrations in molybdenite were determined in the Source Rock and Sulfide Geochronology and Geochemistry Laboratory at the University of Durham, United Kingdom. The details of the analytical techniques are summarized in **Online Resource 1** and the major and trace element data of the Pınarbaşı intrusion are listed in **Online Resources 2 and 3**.

5.1.Whole-rock geochemistry of the Pınarbaşı intrusion

The Pınarbaşı intrusive rocks range in composition from diorite–granodiorite to monzonite with SiO_2 contents varying from 61 to 69 wt.% (**Fig. 6a**). All samples of the Pınarbaşı intrusion straddle the boundary between alkaline and subalkaline series and show a calc-alkaline trend on the AFM diagram (**Figs. 6a-b**). In addition, they belong to the high-K calc-alkaline series on the K_2O vs SiO_2 classification diagram of Peccerillo and Taylor (1976; **Fig. 6c**). The Pınarbaşı samples are also transitional metaluminous to peraluminous based on A/CNK ($Al_2O_3/(CaO+Na_2O+K_2O)$) values varying from 0.9 to 1.2. The porphyritic granite members, i.e. the most evolved samples, of the Pınarbaşı intrusion are mildly peraluminous, whereas the monzonite, and enclave samples are predominantly metaluminous and display similarities with western Aegean Oligo–Miocene felsic intrusions (**Fig. 6d**). On binary plots, the samples show decreasing Al_2O_3, Fe_2O_3, MgO, CaO, TiO_2, and P_2O_5 contents with increasing SiO_2 concentrations. Despite scattered variations, Sr, V, and Zr decrease with increasing SiO_2, whereas Th and Ni display no marked correlation with increasing SiO_2 (**see Online Resource 4**). All samples from the Pınarbaşı intrusion display similar trace element patterns (**Fig. 7a)**. They are enriched in large-ion lithophile elements (LILEs; e.g., Th, K, Ba) and are depleted in high-field strength elements (e.g., Nb, Ta, P, and Ti). Furthermore, they have trace element patterns

similar to those of the upper crust. The Pınarbaşı samples display a pronounced light rare earth element (LREEs) enrichment with respect to middle (MREEs) and heavy rare earth elements (HREEs) (La_N/Yb_N = 10–36, La_N/Gd_N = 7.2–13), with weak to strong negative Eu anomalies (Eu/Eu* = 0.66–0.85), and minor depletion in MREEs (Gd_N/Yb_N = 1.13–1.59) (**Fig. 7b**).

5.2.Whole-rock Sr, Nd, and Pb isotopic compositions

The analytical techniques used in the study are summarized in **Online Resource 1**. Sr, Nd, and Pb isotope ratios for whole-rock samples from Pınarbaşı (granitic and monzonitic) are presented in **Tables 1 and 2**. The age-corrected initial Sr, Nd, and Pb isotopic ratios were calculated for an age of 20 Ma, which is generally accepted for Oligo–Miocene felsic intrusions in the region. The $^{87}Sr/^{86}Sr_{(i)}$ of the porphyritic granite samples range from 0.70774 to 0.70923, whereas the initial Sr isotope ratios of the monzonite and monzodiorite samples range from 0.70718 to 0.70820 (**Table 1**). The $^{143}Nd/^{144}Nd_{(i)}$ ratios of the porphyritic granite samples vary from 0.51234 to 0.51242 (εNd values of −3.85 to −5.38), and the $^{143}Nd/^{144}Nd_{(i)}$ ratios of monzonite and monzodiorite samples vary from 0.51228 to 0.51245 (εNd values of −3.22 to −6.45). A dioritic enclave sample has a $^{87}Sr/^{86}Sr_{(i)}$ ratio of 0.70718 and a $^{143}Nd/^{144}Nd_{(i)}$ ratio of 0.51244 (εNd value of −3.4). The evolved samples from the Pınarbaşı intrusion (Gtk-15 with 68.5 wt.% SiO_2, and Gtk-06 with 68.7 wt.% SiO_2) have higher $^{87}Sr/^{86}Sr_{(i)}$ ratios (0.70923 and 0.70855, respectively) even though there are no significant differences in the $^{143}Nd/^{144}Nd_{(i)}$ ratios (Gtk-06: 68.7 wt.% SiO_2 with 0.51236 $^{143}Nd/^{144}Nd_{(i)}$ ratio and Gtk-09: 61.2 wt.% SiO_2 with 0.51245 $^{143}Nd/^{144}Nd_{(i)}$ ratio) between the most and least evolved samples of the Pınarbaşı. **Figure 8a** shows the initial Sr and Nd isotopic compositions of the samples, the potential source

326 reservoirs, Oligo−Miocene (OMG) and Eocene felsic intrusions (EOG), Simav
327 volcanic rocks (SMV), Baklan felsic intrusions (BG), and Kula volcanic rocks (KV). In
328 the Nd vs Sr isotope space (**Fig. 8a**), the Pınarbaşı intrusion samples fall along an
329 array indicating crustal contamination of mantle-derived melts. The correlation
330 between $^{143}Nd/^{144}Nd_{(i)}$ and $^{87}Sr/^{86}Sr_{(i)}$ ratios is slightly negative and all samples
331 overlap with the compositions of the Eastern Mediterranean Sea Sediments (EMMS),
332 OMG, and SMV (**Fig. 8a**). In contrast, they have higher $^{87}Sr/^{86}Sr_{(i)}$ and $^{143}Nd/^{144}Nd_{(i)}$
333 ratios than those of the BG samples.
334
335 The Pınarbaşı samples yield a relatively restricted range of $^{206}Pb/^{204}Pb_{(i)}$,
336 $^{207}Pb/^{204}Pb_{(i)}$, and $^{208}Pb/^{204}Pb_{(i)}$ ratios (**Figs. 8b-c**). The monzonite and monzodiorite
337 sample ranges are, respectively, 18.935–19.021, 15.716–15.724 and 39.070–39.091,
338 and the porphyritic granite sample ranges are 18.936–18.951, 15.717–15.721 and
339 39.068–39.082, respectively (**Table 2**). A dioritic enclave sample has the least
340 radiogenic $^{206}Pb/^{204}Pb_{(i)}$, $^{207}Pb/^{204}Pb_{(i)}$, and $^{208}Pb/^{204}Pb_{(i)}$ ratios of 18.939, 15.717, and
341 39.065, respectively. All samples plot above the Upper Crust curve (Zartman and
342 Doe 1981) and partly overlap with the compositions of the basement metamorphic
343 rocks, the Eğrigöz granitoid (EG), and the SMV (**Fig. 8b**). In contrast, they have more
344 radiogenic $^{206}Pb/^{204}Pb_{(i)}$, and $^{207}Pb/^{204}Pb_{(i)}$ ratios than the Kula volcanic rocks (KV).
345 On the $^{206}Pb/^{204}Pb_{(i)}$ vs $^{208}Pb/^{204}Pb_{(i)}$ diagram (**Fig. 8c**), they also intersect the EMSS
346 field comprising Sahara desert dust, Nile sediments, and minor Tethyan ophiolitic
347 and arc volcanic rocks from the Hellenic trench, which were traced in Stromboli
348 volcanic rocks along the Aeolian arc (Klaver et al. 2015), and have a less radiogenic
349 $^{208}Pb/^{204}Pb_{(i)}$ ratio compared to basement metamorphic rocks (**Fig. 8c**). In **Figure 8d**,
350 all samples from Pınarbaşı display $^{87}Sr/^{86}Sr_{(i)}$ trending towards the subducted

sediment-rich Enriched Mantle II end member (EM2; Zindler and Hart 1986), the Global Subducted Sediments end member (GLOSS; Plank and Langmuir 1998), and basement metamorphic rocks (MMM, higher radiogenic Sr reservoirs) with nearly constant $^{206}Pb/^{204}Pb_{(i)}$ ratios.

5.3. Molybdenite Re-Os geochronology

The Re-Os age results for two molybdenite samples are presented in **Table 3** and the analytical techniques are summarized in **Online Resource 1**. Two molybdenite samples were selected from an outcrop (OKY-3-4) and a drill core (GOP-19m) from the Pınarbaşı prospect. Sample OKY-3-4 was collected from a molybdenite–hematite bearing silicified zone (**Fig. 4d**), and sample GOP-19m was taken from a 0.5-1cm thick quartz–molybdenite–pyrite–chalcopyrite vein crosscutting a highly sericitized porphyritic granite (**Fig. 4e**). The total Re concentrations of the molybdenite samples are 950 and 1036 ppm and ^{187}Os concentrations are 181 and 199 ppb. Samples OKY-3-4 and GOP-19m yield Re-Os ages of 18.3 ± 0.1 Ma and 18.2 ± 0.1 Ma, respectively (Table 3).

6. Discussion

6.1. Shallow-level magmatic processes

Decreasing CaO, Fe_2O_3, TiO_2, P_2O_5, and V trends with increasing SiO_2 are consistent with pyroxene, apatite, and Fe–Ti oxide fractionation during the evolution of the magmas of the Pınarbaşı intrusion (**see Online Resource 4**), and the fractionated LREE element patterns and slightly negative Eu anomalies indicate plagioclase fractionation during the evolution of the felsic pluton. In addition, the negative correlation of Dy/Yb with SiO_2 (**Fig. 9a**), the positively correlated Zr/Sm ratio

and SiO_2 contents, as well as the slightly upward concave trend from MREEs to HREEs (**Figs. 7b and 9b**) suggest low-pressure amphibole fractionation in the presence of plagioclase. These fractionation trends, coupled with the negative correlation of Al_2O_3, Na_2O, and Sr with SiO_2 are consistent with combined amphibole, plagioclase, and pyroxene fractionation at low pressure, and the absence of high-pressure garnet fractionation and garnet-bearing residue in the source (**see Online Resource 4;** Macpherson et al. 2006; Davidson et al. 2007, 2013; Alonso-Perez et al. 2009; Hora et al. 2009).

The Pınarbaşı samples are characterized by upper continental crust-like lithogeochemical compositions (**Figs. 7a-b**). On the $^{206}Pb/^{204}Pb_{(i)}$ vs $^{207}Pb/^{206}Pb_{(i)}$ diagram (**Fig. 8b**), all Pınarbaşı samples plot above the Upper Crustal curve (Zartman and Doe 1981) and overlap with the basement metamorphic rocks. However, the Sr and Nd isotopic compositions together with A/CNK ratios of 3 to 2 and Mg# values of 30–47 for metamorphic basement (Dilek et al. 2009) are different from those of the metamorphic basement rocks of the region. The high $^{87}Sr/^{86}Sr_{(i)}$ ratios of the evolved samples of porphyritic granite (**Fig. 8a**; **Table 1**) are consistent with upper crustal assimilation concomitant with fractional crystallization (DePaolo 1981). The 1/Sr vs. $^{87}Sr/^{86}Sr_{(i)}$ and SiO_2 vs. $^{208}Pb/^{204}Pb_{(i)}$ plots also show that the porphyritic granite, which crosscuts the Pınarbaşı monzonite, reflects shallow-level crustal assimilation during fractionation (**Figs. 9c-d**). On the $^{206}Pb/^{204}Pb_{(i)}$ vs $^{87}Sr/^{86}Sr_{(i)}$ plot (**Fig. 8d**), the Pınarbaşı samples display a trend with variable $^{87}Sr/^{86}Sr_i$ ratios for nearly constant $^{206}Pb/^{204}Pb_{(i)}$ ratios.

However, several compositional characteristics are attributed to source-inheritance rather than to shallow-level crustal assimilation and fractionation only. They include (1) the least radiogenic Sr compositions (**Fig. 8d**), (2) a low $^{208}Pb/^{204}Pb_{(i)}$ ratio distinct with respect to the metamorphic basement (MMM in **Fig. 8c**), (3) samples with the most radiogenic Nd isotopic compositions (**Fig. 8a**), and (4) enriched U and Pb contents of the Pınarbaşı samples with respect to those of the metamorphic basement (MMM in **Fig. 7a**). In summary, trace element patterns and Pb isotope ratios indicate that the magmas at the origin of the Pınarbaşı intrusion have assimilated middle to upper crustal materials.

6.2 Source of magma

In addition to fractional crystallization and assimilation (AFC) during evolution of the Pınarbaşı magmas, there is geochemical and isotopic evidence for open-system evolution, including partial melting, crust–mantle interaction, and enriched mantle contributions. Partial melting of hydrous calc-alkaline to high-K calc-alkaline, and basaltic to intermediate metamorphic rocks can produce moderate to mildly peraluminous high-K, I-type granitoids (Rapp et al. 1991; Roberts and Clemens 1993; Rudnick and Gao 2003). This can explain the mildly peraluminous composition of the Oligo–Miocene granitic rocks in western Anatolia (**Fig. 6d**), and they are distinct with respect to the composition of metagraywacke and metapelite partial melts (**Fig. 10a**).

The high-K and LILE-enriched (e.g., Ba, Sr) magmas can also be produced from the influx of a LILE- and LREE-enriched- mantle melt at the base of the lower crust, and this source could be produced by small to moderate degrees (≤20%) of partial

melting of phlogopite–clinopyroxene–amphibole-bearing metasomatised lithospheric mantle due to heating by asthenospheric upwelling (Lloyd et al. 1985; Foley 1992; Conticelli et al. 2002; Grove et al. 2003; Condamine and Médard 2014). On the La/Yb vs La diagram (**Fig. 10b)**, the Pınarbaşı samples scatter between the partial melting and fractional crystallization lines, suggesting partial melting of a lithospheric mantle source contemporaneously with fractionation, and the highly variable Nb/Ta ratio of the monzonitic and granitic samples between 7.9 and 34 (~11–12 for crust, and ~17.5 for mantle; Green 1995) indicate fractional crystallization and low degrees of partial melting. In addition, the high Rb/Sr (0.2-0.4) and highly variable Ba/Rb (7.5–18.6) ratios of the Pınarbaşı samples are consistent with partial melting of a residual hydrous phlogopite–amphibole- enriched mantle source (**see Online Resource 2**; Furman and Graham 1999; Guo et al. 2013). The low Sm/Yb ratio below 3 of the Pınarbaşı granitic and monzonitic samples (**Fig. 10c**) suggests a residue above the garnet stability field at 35–40 km (Kay and Mpodozis 2001). The position of all samples in the mantle–crust interaction field in the Nb–Y–Ga*3 ternary diagram of Eby (1992) (**Fig. 10d**) is consistent with phlogopite–amphibole–pyroxene-bearing lithospheric mantle-lower crust interactions.

Based on our geochemical data, the absence of residual garnet in the magma source reflects a relatively thin crust in mid-western Anatolia since at least the Oligo–Miocene. Geophysical data document a present-day average crustal thickness of 25 to 33 km in western Anatolia, and an average crustal thickness of 40 km during the early Miocene (Dhont et al. 2006; Mutlu and Karabulut 2011; Karabulut et al. 2013). Consequently, our results coupled with the crustal thickness of western Anatolia allow us to conclude that enriched sub-continental lithospheric mantle interacted with

451 the lower crust and generated the parental magmas of the Oligo–Miocene granitic
452 intrusions at relatively low pressure (35–40 km).
453
454 *6.3. Post-subduction tracers*
455 Enrichment of LILEs (e.g., Ba, Rb, Sr), U and Pb, depletion of Nb and Ta, and high
456 Ba/La, Ba/Th, Rb/Y, Sr/Th and Sr/Nd ratios are attributed to fluid addition to the
457 mantle wedge from dehydration of a subducted slab (Pearce and Peate 1995;
458 Keppler 1996). By contrast, enrichment of Th, La, and Nb are attributed to
459 metasomatism of the mantle by melting of a subducted sedimentary component
460 (Tatsumi et al. 1986; Plank and Langmuir 1993; Brenan et al. 1995; Pearce and
461 Peate 1995; Plank 2005).
462
463 All samples of the Pınarbaşı intrusion, together with the Oligo-Miocene granitic rocks
464 of the western Aegean, exhibit variable Th/Yb ratios for nearly constant Ta/Yb ratios
465 (**Fig. 11a**), and reflect a subduction-related environment. The wide range of Ba (666–
466 2100 ppm), Sr (333–621 ppm) contents and high Ba/La (17.7–42.6) ratios of the
467 Pınarbaşı samples are consistent with addition of aqueous fluids derived from the
468 mantle wedge to the sub-lithospheric mantle. A narrow range of Nb/Y ratio with highly
469 variable Ba contents could also be attributed to slab-derived fluid enrichment (**Fig.**
470 **11b**). On the other hand, the relatively high Th/La (0.33–0.73), Th/Nb (1.0–2.3), Zr/Hf
471 (33.4–41.9, Zr/Hf = ~39.6 for EMSS) and a wide range of Th/Yb ratios (5.2–13.6;
472 excluding the high Th/Yb ratio of 31 of sample GOTK-18), as well as the low Ce/Pb
473 ratios (1.35–3.84; Ce/Pb = ~3.98 for EMSS and Ce/Pb = 2–3 for terrigenous
474 sediments; Lan et al. 1990; Klaver et al. 2015), with small negative Ce anomalies of
475 Pınarbaşı granitic and monzonitic rocks (**Fig. 7a)** could be indicative of a sedimentary

476 component mixed with an enriched mantle source. In the Nb/Y vs. Rb/Y plot (**Fig.**
477 **11c**), the Pınarbaşı samples exhibit a trend between melt-related enrichment and
478 slab-derived fluid enrichment array lines. These metasomatic agents are further
479 documented by the oblique trend between fluid- and melt-related enrichment trend
480 lines on the Th/Nb vs. Ba/Th plot (**Fig. 11d**) and also on the Ba/La vs Th/Yb plot (**Fig.**
481 **11e**). They have higher Ba/Nb and Th/Nb ratios than the EMSS and on the Th/Nb vs.
482 Ba/Nb diagram (**Fig. 11f**), they lie along both the sediment melting and aqueous fluid
483 trend lines. It is known that wet sediment melting can only occur at depths greater
484 than 100 km under relatively high temperatures (~800 °C) and the increased K, Th,
485 Ta, and Nb concentrations in arc-suites are attributed to the distance from the
486 subduction trenches, reflecting the heterogeneous mantle sources that change from
487 subduction-related to within-plate away from the trench and the low degree of partial
488 melting in the back-arc setting also leads to enrichment in incompatible elements
489 (Barragan et al. 1998; Aizawa et al. 1999; Duggen et al. 2007; Richards 2011; Müller
490 and Groves 2016). Therefore, the enrichment processes can be linked with
491 magmatism related to back-arc opening in the region as a consequence of hot
492 asthenospheric upwelling attributed either to slab rollback and subsequent slab tear
493 processes (Spakman et al. 1988; Jolivet and Brun 2010; van Hinsbergen 2010; Erkül
494 et al. 2013; Ersoy and Palmer 2013; Jolivet et al. 2013, 2015) or lithospheric
495 delamination and convective thinning of the lithospheric mantle (Dilek et al. 2009;
496 Altunkaynak et al. 2012a).
497
498 *6.4. Age of Mo-Cu Mineralization*
499 The early Miocene crystallization ages of molybdenite from the stockwork veins (18.3
500 ± 0.1 Ma and 18.2 ± 0.1 Ma) coincide with the crystallization and cooling ages of the

granitic rocks of the Oligo-Miocene magmatic pulse in western Anatolia (**Fig. 12**; ~24.0 and 18 Ma; Isik et al. 2004; Ring and Collins 2005; Aydoğan et al., 2008; Hasözbek et al. 2010; Altunkaynak et al. 2012a). This indicates a very close relationship of the mineralization event with the latest magmatic differentiation, crystallization and subsequent cooling stages. In addition, the early Miocene age of the Mo-Cu mineralization at Pınarbaşı shows that metal enrichment was closely related to early Miocene post-orogenic magmatism **(Fig. 12).**

6.5. Origin of metals in the porphyry-style Mo–Cu Pınarbaşı prospect

The trace element data and the Sr, Nd, and Pb isotopic compositions of the Pınarbaşı intrusive rocks suggest that the Mo–Cu-bearing monzonitic and granitic rocks were derived from a melt that was produced by interaction of an enriched, metasomatised lithospheric mantle and a lower crust at a depth of 35–40 km during the Oligo–Miocene. The enriched melt influx from the metasomatised lithospheric mantle into the lower crust resulted in partial melting of the lower crust at the lithospheric mantle–lower crust interface. Lithospheric mantle interaction with the lower crust likely increased through time, and lithospheric influx during the mid to late Miocene probably resulted in thickening of the lower crust in western Anatolia (see also discussion by Ersoy et al. 2010). This is consistent with the evolution of Oligo–Miocene high-K calc-alkaline to middle Miocene shoshonitic magmatism in the region interpreted as deep partial melting (Thorpe and Francis 1979). It is also in line with the formation of an amphibole–garnet-bearing residual source during early to middle Miocene magmatism (e.g., Ersoy et al. 2010; Çoban et al. 2012; Karaoğlu and Helvacı 2014).

Commented [A1]: The second part of this section discusses the origin of the metals. Therefore, it's probably best to keep this title as proposed by Okan.

Continuous partial melting of chalcophile and siderophile element-enriched lower crustal amphibolitic cumulates and sub-continental lithospheric mantle can produce H_2O-bearing, volatile-rich and fertile melts, which are the source of metals of porphyry Au-Cu deposits in post-collisional extensional settings (Richards 2009; Hou et al. 2011; Richards and Mumin 2013; Hou and Zhang 2014; Müller and Groves 2016). The crustal or mantle origin of the Mo-enrichment in porphyry systems is still debated (Audétat 2010; Richards 2011). Pettke et al. (2010) advocated melting for sub-continental metasomatised old mantle as the source of Mo for giant porphyry Mo-rich systems in the Western U.S.A., and Mao et al (2011) suggested that repeated melting of the lower crust can explain Mo-enrichment in back-arc extensional settings during post-collisional magmatism. Molybdenum is enriched in reduced sediments and is also immobile in low-temperature fluids (Crusius et al. 1996). Chondritic to super-chondritic ratios of Zr/Hf (33–42) and Hf/Sm (0.75–1.04) of the Pınarbaşı intrusion reveal a terrigenous character of the subducted crustal material (chondritic value of Hf/Sm: 0.75; Zr/Hf: 35–40, Patchett et al. 2004, Claiborne et al. 2006). Therefore, our study reveals that melting of terrigenous sediments can also supply Mo to an enriched lithospheric mantle source in a back-arc setting. In light of these studies, it is concluded that a lithospheric mantle metasomatised by fluids and subducted sediments, interacting at relatively low-pressure conditions (depths of 35–40 km) with lower crust could explain the Mo–Cu enrichment of the Pınarbaşı intrusion during back-arc magmatism (**Fig. 12**). The over-thickened sub-continental lithospheric mantle during early to late Miocene could have created the adequate environment for the evolution of larger scale Au ± Cu ± Mo-rich deposits in western Anatolia (e.g., middle Miocene Uşak-Afyon-Konya

district, Kuşçu et al. 2011; Rabayrol et al 2014), because of continuous melting of chalcophile and siderophile element-enriched amphibolite cumulates in the thickened lower crust and the enriched lithospheric mantle.

6.6. Tectonic setting, exhumation and epithermal overprint of the porphyry Mo–Cu Pınarbaşı prospect

Extensional tectonics favors the migration of highly oxidized, Cu–, Au– and Mo-rich melts derived from the mantle and the lower crust into upper crustal levels (Vigneresse 2007). The ore-bearing melt at the origin of the Pınarbaşı intrusion could have rapidly ascended to mid-crustal levels with crustal assimilation along trans-lithospheric faults activated during extension, and resulting in porphyry-style Mo-Cu mineralization during the early Miocene (at ~18 Ma) that is consistent with the differentiation-crystallization and cooling history of the Oligo-Miocene granites (24-18 Ma). The first, late Oligocene to early Miocene phase of extension in the region is mainly characterized by the development of low-angle shear zones and the subsequent emplacement and exhumation of granitic rocks along the ductile shear zones (**Fig. 12**). Hence, the Oligo–Miocene felsic intrusions are regarded as syn-extensional, that cooled rapidly along the footwall of detachment faults (Ring et al. 2003; Isik et al. 2004; Ring and Collins 2005; Dilek et al. 2009; Erkül 2010). The second, middle to late Miocene extension phase in the region is characterized by the development of high-angle normal faults forming graben structures in western Anatolia (Yilmaz 1989; Hetzel et al. 1995; Ring et al. 2003; **Fig. 12**). The high-angle normal faulting resulted in uplift of the graben shoulders, deep erosion and further exhumation along the detachment footwalls, as well as cataclastic deformation of the Oligo–Miocene granitic rocks (Yilmaz 1989; Dilek et al. 2009). Therefore, exhumation

of the Mo–Cu-bearing Pınarbaşı intrusion, exposed in the northwestern shoulder of the Yenidoğmuş–YeniGediz graben, can be explained by uplift of the graben systems (**Fig. 2**, **inset**). Further uplift during the middle to late Miocene may have resulted in (1) removal of the shallow parts of the Pınarbaşı porphyry system in response to rapid erosion, (2) telescoping by Sb±Ag±Au low-sulfidation epithermal mineralization, and intense advanced argillic alteration at the Pınarbaşı prospect (**Figs. 5e-f**; Oygür and Erler 2000; Delibas et al. 2012a). This is reminiscent of many porphyry systems in post-collisional extensional settings (e.g., Perello et al. 2001; Hou et al. 2009).

7. Conclusions

The high-K calc-alkaline Pınarbaşı intrusion shares many geochemical features with other calc-alkaline to high-K calc-alkaline Oligo–Miocene granitic rocks of western Anatolia. The monzonitic and granitic rocks of Pınarbaşı were derived from interactions of an enriched lithospheric mantle and lower crust at depth of 35–40 km during Oligo–Miocene post-collisional magmatism. Trace-element ratios and distinct Sr, Nd, and Pb isotopic compositions of the Pınarbaşı intrusion suggest that two metasomatic agents could have been incorporated into the enriched mantle source reflecting post-orogenic magmatism. We conclude that the lithospheric mantle was metasomatised by fluids and subducted sediments, and its interaction with a lower crust at low-pressure conditions explains the Mo and Cu enrichment of the Pınarbaşı intrusion during back-arc magmatism. The ore-bearing melt of the Pınarbaşı intrusion could have rapidly ascended to mid-crustal levels, with only limited crustal assimilation along major trans-lithospheric faults as a result of the thinning of middle to upper crust during regional extension, and resulted in the development of porphyry-style mineralization during the early Miocene (~18 Ma). The subsequent

exhumation history of the Mo–Cu-bearing Pınarbaşı intrusion is attributed to regional-scale uplift, and further exhumation along the detachment faults of the associated core complexes during the middle to late Miocene. This evolution also resulted in an overprint by epithermal mineralization, and intense advanced argillic alteration.

Acknowledgments

The authors would like to thank Fabio Capponi for XRF analyses (University of Geneva*)* and Peter Laznicka (Metallogenica Consulting Adelaide), Cüneyt Baran, Fatih Pekdemir, and Oktay Parlak (MTA) for help during fieldwork. Panagiotis Voudouris and Albrecht von Quadt are thanked for their valuable comments and suggestions that allowed us to improve the manuscript. We also thank associated editor Frank Melcher for final edits. The research was supported by the "*Hacettepe University Scientific Research Coordination Unit*" grants FHD-2015-7509 and FDS-2015-7004, and *the "Swiss National Science Foundation"* through research grants 200020-155928. This research was also partially supported by the General Directorate of Mineral Research and Exploration, Turkey (MTA)–*ETI Mine Works* during the joint project 2002-32-57.d1. David Selby acknowledges the TOTAL endowment fund. Seçil Delibaş and Burcu Kahraman (Hacettepe University) are thanked for providing various pieces of information allowing us to finalize the manuscript. This paper is dedicated to the memory of the senior author Okan Delibaş, who dramatically passed away in August 2016 during the final revision stages of the manuscript. Okan still had so many scientific projects in mind, his death is a big loss to all of us, including his family, friends, colleagues and the international scientific community.

626 **References**

627 Aghazadeh M, Hou Z, Badrzadeh Z, Zhou L (2015) Temporal–spatial distribution and
628 tectonic setting of porphyry copper deposits in Iran: Constraints from zircon U–Pb
629 and molybdenite Re–Os geochronology. Ore Geol Rev 70: 385-406

630 Agostini S, Doglioni C, Innocenti F, Manetti P, Tonarini S, Savaşçın M (2007) The
631 transition from subduction-related to intraplate Neogene magmatism in the Western
632 Anatolia and Aegean area. In Beccaluva L, Bianchini G, Wilson M (eds) Cenozoic
633 Volcanism in the Mediterranean Area. Geol Soc Am Spec Paper 418: 1–15

634 Agostini S, Doglioni C, Innocenti F, Manetti P, Tonarini, S (2010) On the
635 geodynamics of the Aegean rift. Tectonophysics 488: 7–21
636 Aizawa Y, Tatsumi Y, Yamada H (1999) Element transport by dehydration of
637 subducted sediments: Implication for arc and ocean island magmatism. Isl Arc 8: 38–
638 46
639
640 Akdeniz N, Konak N (1979) Geology of the Simav-Emet-Tavşanlı-Dursunbey-Demirci
641 region. Report, General Directorate of Mineral Research and Exploration, Turkey
642 (MTA) Report No: 6547, Ankara (unpublished, in Turkish)
643
644 Aldanmaz E, Pearce JA, Thirlwall MF, Mitchell, JG (2000) Petrogenetic evolution of
645 late Cenozoic, post-collision volcanism in western Anatolia, Turkey. J Volcanol Geoth
646 Res 102: 67–95
647
648 Alici P, Temel A, Gourgaud A (2002) Pb-Nd-Sr isotope and trace element
649 geochemistry of Quaternary extension-related alkaline volcanism: A case study of

650 Kula region (western Anatolia, Turkey). J Volcanol Geoth Res 115: 487–510
651
652 Alonso-Perez R, Müntener O, Ulmer P (2009) Igneous garnet and amphibole
653 fractionation in the roots of island arcs: Experimental constraints on andesitic liquids.
654 Contrib Mineral Petr 157: 541–558
655
656 Altunkaynak Ş, Dilek Y (2006) Timing and nature of postcollisional volcanism in
657 western Anatolia and geodynamic implications. In Dilek Y, Pavlides, S (eds)
658 Postcollisional tectonics and magmatism in the Mediterranean region and Asia. Geol
659 Soc Am Spec Paper 409: 321–351
660
661 Altunkaynak Ş, Dilek Y, Genç CŞ, Sunal G, Gertisser R, Furnes H, Foland KA, Yang,
662 J (2012a) Spatial, temporal and geochemical evolution of Oligo-Miocene granitoid
663 magmatism in western Anatolia, Turkey. Gondwana Res 21: 961–986
664
665 Altunkaynak Ş, Sunal G, Aldanmaz E, Genç CŞ, Dilek Y, Furnes H, Foland, KA,
666 Yang J, Yildiz M (2012b) Eocene granitic magmatism in NW Anatolia (Turkey)
667 revisited: New implications from comparative zircon SHRIMP U-Pb and $^{40}Ar/^{39}Ar$
668 geochronology and isotope geochemistry on magma genesis and emplacement.
669 Lithos 155: 289–309
670
671 Arikas K, Voudouris P (1998) Hydrothermal alterations and mineralizations of
672 magmatic rocks in the southeastern Rhodope Massif. Acta Vulcanologica 10: 353-
673 365
674

675 Audetat A (2010) Source and evolution of molybdenum in the porphyry Mo(-Nb)
676 deposit at Cave Peak, Texas. J Petrol 51: 1739–1760
677
678 Aydoğan MS, Çoban H, Bozcu M, Akinci Ö (2008) Geochemical and mantle-like
679 isotopic (Nd, Sr) composition of the Baklan Granite from the Muratdağı Region
680 (Banaz, Uşak), western Turkey: Implications for input of juvenile magmas in the
681 source domains of western Anatolia Eocene-Miocene granites. J Asian Earth Sci 33:
682 155–176
683
684 Barragan R, Geist D, Hall M, Larson P, Kurz M (1998) Subduction controls on the
685 compositions of lavas from the Ecuadorian Andes. Earth Planet Sci Lett 154: 153-
686 166
687
688 Bozkurt E (2004) Granitoid rocks of the southern Menderes Massif (southwestern
689 Turkey): field evidence for Tertiary magmatism in an extensional shear zone. Int J
690 Earth Sci 93: 52–71
691
692 Bozkurt E, Park RG (1997) Evolution of a mid-Tertiary extensional shear zone in the
693 southern Menderes Massif, western Turkey. Bull Soc Geol France 168: 3–14
694
695 Bozkurt E, Sözbilir H (2004) Tectonic evolution of the Gediz Graben: field evidence
696 for an episodic, two-stage extension in western Turkey. Geol Mag 141: 63–79
697
698 Bozkurt E, Park RG, Winchester JA (1993) Evidence against the core/cover
699 interpretation of the southern sector of the Menderes Massif, west Turkey. Terra

700 Nova 5: 445–451
701
702 Brenan JM, Shaw HF, Ryerson FJ, Phinney DL (1995) Mineral-aqueous fluid
703 partitioning of trace elements at 900°C and 2.0 GPa: Constraints on the trace
704 element chemistry of mantle and deep crustal fluids. Geochim Cosmochim Acta 59:
705 3331–3350
706
707 Candan O, Çetinkaplan M, Oberhänsli R, Rimmelé G, Akal C (2005) Alpine high-
708 P/low-T metamorphism of the Afyon Zone and implications for the metamorphic
709 evolution of Western Anatolia, Turkey. Lithos 84: 102–124
710
711 Chiaradia M, Muntener O, Beate B (2011) Enriched basaltic andesites from mid-
712 crustal fractional crystallization, recharge, and assimilation (Pilavo Volcano, western
713 Cordillera of Ecuador). J Petrol 52: 1107–1141
714
715 Chakrabarti R, Basu, AR, Ghatak A (2012) Chemical geodynamics of Western
716 Anatolia. Int Geol Rev 54: 227–248
717
718 Claiborne L, Miller CF, Walker BA, Wooden JL, Mazdab FK, Bea F (2006) Tracking
719 magmatic processes through Zr/Hf ratios in rocks and Hf and Ti zoning in zircons: An
720 example from the Spirit Mountain batholith, Nevada. Mineral Mag 70: 517–543
721
722 Collins AS, Robertson AHF (1997) Lycian melange, southwestern Turkey: An
723 emplaced Late Cretaceous accretionary complex. Geology 25: 255–258
724

725 Condamine P, Médard E (2014) Experimental melting of phlogopite-bearing mantle
726 at 1 GPa: Implications for potassic magmatism. Earth Planet Sci Lett 397: 80–92
727
728 Conticelli S, Antonio MD, Pinarelli L, Civetta L, Federico N (2002) Source
729 contamination and mantle heterogeneity in the genesis of Italian potassic and
730 ultrapotassic volcanic rocks : Sr-Nd-Pb isotope data from Roman Province and
731 Southern Tuscany. Mineral Petrol 74: 189–222
732
733 Crusius J, Calvert S, Pedersen T, Sage D (1996) Rhenium and molybdenum
734 enrichments in sediments as indicators of oxic, suboxic and sulfidic conditions of
735 deposition. Earth Planet Sci Lett 145: 65–78
736
737 Çoban H, Karacik Z, Ece ÖI (2012) Source contamination and tectonomagmatic
738 signals of overlapping Early to Middle Miocene orogenic magmas associated with
739 shallow continental subduction and asthenospheric mantle flows in Western Anatolia:
740 A record from Simav (Kütahya) region. Lithos 140-141: 119–141
741
742 Davidson J, Turner S, Handley HK, Macpherson C, Dosseto A (2007) Amphibole
743 “sponge” in arc crust? Geology 35: 787–790
744
745 Davidson J, Turner S, Plank T (2013) Dy/Dy*: Variations arising from mantle sources
746 and petrogenetic processes. J Petrol 54: 525–537
747 Delaloye M, Bingöl E (2000) Granitoids from Western and Northwestern Anatolia:
748 Geochemistry and Modeling of Geodynamic Evolution. Int Geol Rev 42: 241–268
749

750 Delibaş O, Parlak O, Pekdemir F, Baran C (2012a) The Pınarbaşı granitoid (Gediz-
751 Kütahya) Mo-Cu, Pb-Zn and Sb±Ag mineralizations: an example of the polymetallic
752 mineralizations from the Mid-West Anatolia. Yerbilimleri 33: 151–176 (in Turkish)
753
754 Delibaş O, Baran C, Pekdemir F (2012b) Pınarbaşı (Kütahya-GedizGediz) region
755 2010-2011 mineral expoloration and ore geology report. General Directorate of
756 Mineral Research and Exploration, Turkey (MTA). Report No: 6580, Ankara
757 (unpublished, in Turkish)
758
759 DePaolo DJ (1981) Trace element and isotopic effects of combined wallrock
760 assimilation and fractional crystallization. Earth Planet Sci Lett 53: 189–202
761
762 Dhont D, Chorowicz J, Luxey P (2006) Anatolian escape tectonics driven by Eocene
763 crustal thickening and Neogene–Quaternary extensional collapse in the eastern
764 Mediterranean region. In Dilek Y, Pavlides, S (eds) Postcollisional tectonics and
765 magmatism in the Mediterranean region and Asia. Geol Soc Am Spec Paper 409:
766 441–462
767
768 Dilek Y (2006) Collision tectonics of the Mediterranean region: causes and
769 consequences. In: Dilek Y, Pavlides S (eds) Postcollisional tectonics and magmatism
770 in the Mediterranean Region and Asia. Geol Soc Am Spec Paper 409: 1-13
771
772 Dilek Y, Sandvol E (2009) Seismic structure, crustal architecture and tectonic
773 evolution of the Anatolian-African plate boundary and the Cenozoic orogenic belts in
774 the Eastern Mediterranean region. In Murphy JB, Keppie JD, Hynes AJ (eds) Ancient

775 orogens and modern analogues. Geol Soc London Spec Pub 327: 127–160
776
777 Dilek Y, Altunkaynak Ş (2010) Geochemistry of Neogene–Quaternary alkaline
778 volcanism in western Anatolia, Turkey and implications for the Aegean mantle. Int
779 Geol Rev 52: 631–655
780
781 Dilek Y, Altunkaynak Ş, Oner Z (2009) Syn-extensional granitoids in the Menderes
782 core complex and the late Cenozoic extensional tectonics of the Aegean province. In
783 Ring U, Wernicke B (eds) Extending a continent: Architecture, rheology and heat
784 budget. Geol Soc London Spec Pub 321: 197–223
785
786 Doglioni C, Agostini S, Crespi M, Innocenti F, Manetti P, Riguzzi F, Savaşçın MY
787 (2002) On the extension in western Anatolia and the Aegean sea. In Rosenbaum G,
788 Lister GS (eds) India-Asia convergence in NW Himalaya: Reconstruction of the
789 evolution of the Alpine-Himalayan Orogen. J Virtual Explor 7: 167–181
790
791 Duggen S, Portnyagin M, Baker J, Ulfbeck D, Hoernle K, Garbe-Schönberg D,
792 Grassineau N (2007) Drastic shift in lava geochemistry in the volcanic-front to rear-
793 arc region of the Southern Kamchatkan subduction zone: Evidence for the transition
794 from slab surface dehydration to sediment melting. Geochim Cosmochim Acta 71:
795 452–480
796
797 Eby GN (1992) Chemical subdivision of the A-type granitoids: Petrogenetic and
798 tectonic implications. Geology 20: 641–644
799

800 Erkül F (2010) Tectonic significance of synextensional ductile shear zones within the
801 Early Miocene Alaçamdağ granites, northwestern Turkey. Geol Mag 147: 611–637
802
803 Erkül ST, Erkül F (2012) Magma interaction processes in syn-extensional granitoids:
804 The Tertiary Menderes metamorphic core complex, western Turkey. Lithos 142-143:
805 16–33
806
807 Erkül F, Erkül ST, Ersoy Y, Uysal I, Klötzli, U (2013) Petrology, mineral chemistry and
808 Sr-Nd-Pb isotopic compositions of granitoids in the central Menderes metamorphic
809 core complex: Constraints on the evolution of Aegean lithosphere slab. Lithos 180-
810 181: 74–91
811
812 Ersoy EY, Palmer MR (2013) Eocene−Quaternary magmatic activity in the Aegean:
813 Implications for mantle metasomatism and magma genesis in an evolving orogeny.
814 Lithos 180-181: 5-24
815
816 Ersoy EY, Helvacı C, Palmer MR (2010) Mantle source characteristics and melting
817 models for the early-middle Miocene mafic volcanism in Western Anatolia:
818 Implications for enrichment processes of mantle lithosphere and origin of K-rich
819 volcanism in post-collisional settings. J Volcanol Geoth Res 198: 112–128
820
821 Foley S (1992) Potassic and ultrapotassic magmas and their origin vein-plus-wall-
822 rock melting mechanisms in the lithosphere and the origin of potassic alkaline
823 magmas. Lithos 28: 435–453
824

825 Furman T, Graham D (1999) Erosion of lithospheric mantle beneath the East African
826 Rift system: geochemical evidence from the Kivu volcanic province. Lithos 48: 237–
827 262
828
829 Fytikas M, Innocenti F, Manetti P, Peccerillo A, Mazzuoli R, Villari L (1984) Tertiary to
830 Quaternary evolution of volcanism in the Aegean region. In Dixon JE, Robertson AHF
831 (eds), The geological evolution of the Eastern Mditerranean Geol Soc London Spec
832 Pub 17: 687–699
833
834 Green TH (1995) Significance of Nb/Ta as an indicator of geochemical processes in
835 the crust-mantle system. Chem Geol 120: 347–359
836
837 Grove TL, Elkins-Tanton L, Parman SW, Chatterjee N, Müntener O, Gaetani GA
838 (2003) Fractional crystallization and mantle-melting controls on calc-alkaline
839 differentiation trends. Contrib Mineral Petr 145: 515–533
840
841 Gökce A, Spiro B (1994) Stable isotope study of antimony deposits in the Muratdağı
842 Region, Western Turkey. Miner Deposita 29: 361-365
843
844 Guo Z, Wilson M, Zhang M, Cheng Z, Zhang L (2013) Post-collisional, K-rich mafic
845 magmatism in south Tibet: Constraints on Indian slab-to-wedge transport processes
846 and plateau uplift. Contrib Mineral Petr 165: 1311–1340
847
848 Güleç N (1991) Crust–mantle interaction in western Turkey: implications from Sr and
849 Nd isotope geochemistry of Tertiary and Quaternary volcanics. Geol Mag 128: 417–

850 435

851

852 Gürboğa Ş, Koçyiğit A, Ruffet G, Koçyiğit A, Ruffet G (2013) Episodic two-stage
853 extensional evolutionary model for southwestern Anatolian graben-horst system:
854 New field data from the Erdoğmuş-Yenigediz graben (Kütahya). J Geodyn 65: 176–
855 198

856

857 Harris NB, Kelley S, Okay A (1994) Post-collision magmatism and tectonics in
858 northwest Anatolia. Contrib Mineral Petr 117: 241–252

859

860 Hasözbek A, Akay E, Erdogan B, Satir M, Siebel W (2010) Early Miocene granite
861 formation by detachment tectonics or not? A case study from the northern Menderes
862 Massif (Western Turkey). J Geodyn 50: 67–80

863

864 Helvacı C, Ersoy Y, Sözbilir H, Erkül F, Sümer Ö, Uzel B (2009) Geochemistry and
865 $^{40}Ar/^{39}Ar$ geochronology of Miocene volcanic rocks from the Karaburun Peninsula:
866 implications for amphibole-bearing lithospheric mantle source, Western Anatolia. J
867 Volcanol Geoth Res 185: 181–202

868

869 Hetzel R, Ring U, Akal C., Troesch M (1995) Miocene NNE-directed extensional
870 unroofing in the Menderes Massif, southwestern Turkey. J Geol Soc London 152:
871 639–654

872

873 Hofmann AW (1997) Mantle geochemistry: the message from oceanic volcanism.
874 Nature 385: 219–229

875

876 Hora JM, Singer BS, Wörner G, Beard BL, Jicha BR, Johnson CM (2009) Shallow
877 and deep crustal control on differentiation of calc-alkaline and tholeiitic magma. Earth
878 Planet Sci Lett 285: 75–86

879

880 Hou Z, Zhang H (2014) Geodynamics and metallogeny of the eastern Tethyan
881 metallogenic domain. Ore Geol Rev 70: 346-384

882

883 Hou Z, Yang Z, Qu X, Meng X, Li Z, Beaudoin G, Rui Z, Gao Y, Zaw K (2009) The
884 Miocene Gangdese porphyry copper belt generated during post-collisional extension
885 in the Tibetan Orogen. Ore Geol Rev 36: 25–51

886

887 Hou Z, Zhang H, Pan X, Yang Z (2011) Porphyry Cu(-Mo-Au) deposits related to
888 melting of thickened mafic lower crust: Examples from the eastern Tethyan
889 metallogenic domain. Ore Geol Rev 39: 21–45

890

891 Innocenti F, Agostini S, Di Vincenzo G, Doglioni C, Manetti P, Savaşçın MY, Tonarini
892 S (2005) Neogene and Quaternary volcanism in Western Anatolia: magma sources
893 and geodynamic evolution. Mar Geol 221: 97–421

894

895 Isik V, Tekeli O, Seyitoglu G (2004) The $^{40}Ar/^{39}Ar$ age of extensional ductile
896 deformation and granitoid intrusion in the northern Menderes core complex:
897 Implications for the initiation of extensional tectonics in western Turkey. J Asian Earth
898 Sci 23: 555–566

899

900 Jackson SE (2008) Lamtrace data reduction software for LA-ICP-MS. In Sylvester P
901 (ed) Laser Ablation ICP-MS in the Earth sciences: Current practices and outstanding
902 issues. Mineral Ass Canada Short Course 40: 305–307
903
904 Jacobsen SB, Wasserburg GJ (1984) Sm–Nd isotopic evolution of chondrites and
905 achondrites. Earth Planet Sci Lett 67: 137–150
906
907 Jolivet L, Brun JP (2010) Cenozoic geodynamic evolution of the Aegean. Int J Earth
908 Sci 99: 109–138
909
910 Jolivet L, Faccenna C, Goffe B, Burov E, Agard P (2003) Subduction tectonics and
911 exhumation of high-pressure metamorphic rocks in the Mediterranean orogens. Am J
912 Sci 303: 353–409
913
914 Jolivet L, Faccenna C, Huet B, Labrousse L, Le Pourhiet L, Lacombe O, Lecomte E,
915 Burov E, Denèle Y, Brun JP, Philippon M, Paul A, Salaün G, Karabulut H, Piromallo
916 C, Monié P, Gueydan F, Okay A, Oberhänsli R, Pourteau A, Augier R, Gadenne L,
917 Driussi O (2013) Aegean tectonics: Strain localisation, slab tearing and trench
918 retreat. Tectonophysics 597-598: 1–33
919
920 Jolivet L, Menant A, Sternai P, Rabillard A, Arbaret L, Augier R, Laurent V, Beaudoin
921 A, Grasemann B, Huet B, Labrousse L, Le L (2015) The geological signature of a
922 slab tear below the Aegean. Tectonophysics 659: 166–182
923
924

925 Kaiser-Rohrmeier M, von Quadt A, Driesner T, Heinrich CA, Handler R, Ovtcharova
926 M, Ivanov Z, Petrov P, Sarov S, Peytcheva I (2013) Post-orogenic extension and
927 hydrothermal ore formation: High-precision geochronology of the central Rhodopian
928 metamorphic core complex (Bulgaria-Greece). Econ Geol 108: 691–718
929
930 Karabulut H, Paul A, Afacan ET, Hatzfeld D, Childs DM, Aktar M (2013) Long-
931 wavelength undulations of the seismic Moho beneath the strongly stretched Western
932 Anatolia. Geophys J Int 194: 450–464
933
934 Karaoğlu Ö, Helvacı C (2014) Isotopic evidence for a transition from subduction to
935 slab-tear related volcanism in western Anatolia, Turkey. Lithos 192-195: 226–239
936
937 Karaoğlu Ö, Helvacı C, Ersoy EY (2010) Petrogenesis and $^{40}Ar/^{39}Ar$ geochronology
938 of the volcanic rocks of the Uşak–Güre basin, western Turkey. Lithos 119: 193–210
939
940 Kay S, Mpodozis C (2001) Cenrtal Andean ore deposits linked to evolving shallow
941 subduction systems and thickening crust. Geol Soc Am Today 11: 4-9
942
943 Keppler H (1996) Constraints from partitioning experiments on the composition of
944 subduction-zone fluids. Nature 380: 237-240
945
946 Klaver M, Djuly T, de Graaf S, Sakes A, Wijbrans J, Davies G, Vroon P (2015)
947 Temporal and spatial variations in provenance of Eastern Mediterranean Sea
948 sediments: Implications for Aegean and Aeolian arc volcanism. Geochim Cosmochim
949 Acta 153: 149–168

Koçyiğit A, Unay E, Sarac G (2000) Episodic graben formation and extensional neotectonic regime in west-central Anatolia and the Isparta angle: A case study in the Aksehir-Afyon graben, Turkey. In Bozkurt E, Winchester JA, Piper JDA (eds) Tectonics and magmatism in Turkey and surrounding area, Geol Soc London Spec Pub 173: 405–421

Koprubasi N, Aldanmaz E (2004) Geochemical constraints on the petrogenesis of Cenozoic I-type granitoids in northwest Anatolia, Turkey: Evidence for magma generation by lithospheric delamination in a post-collisional setting. Int Geol Rev 46: 705–729

Kroll T, Muller D, Seifert T, Herzig PM, Schneider A (2002) Petrology and geochemistry of the shoshonite-hosted Skouries porphyry Cu-Au deposit, Chalkidiki, Greece. Miner Deposita 37: 137–144

Kuşçu İ, Gençalioğlu-Kuşçu G, Tosdal R, Ulrich T, Freidman R (2011) The geochronolgy of gold-copper deposition and temporal association with magmatic rocks in western Anatolia. 64th Geological Congress of Turkey, Ankara, April 25-29, 2011. Abstracts book: 189-190

Lan CY, Lee T, Wang Lee C (1990) The Rb-Sr isotopic record in Taiwan gneisses and its tectonic implication. Tectonophysics 183: 129-143

975 Lloyd FE, Arima M, Edgar AD (1985) Partial melting of a phlogopite-clinopyroxenite
976 nodule from south-west Uganda: an experimental study bearing on the origin of
977 highly potassic continental rift volcanics. Contrib Mineral Petr 91: 321–329
978
979 Macpherson CG, Dreher ST, Thirlwall MF (2006) Adakites without slab melting: High
980 pressure differentiation of island arc magma, Mindanao, the Philippines. Earth Planet
981 Sci Lett 243: 581–593
982
983 Mao JW, Pirajno F, Xiang JF, Gao JJ, Ye HS, Li YF, Guo BJ (2011) Mesozoic
984 molybdenum deposits in the east Qinling-Dabie orogenic belt: Characteristics and
985 tectonic settings. Ore Geol Rev 43: 264–293
986
987 Marchev P, Kaiser-Rohrmeier B, Heinrich C, Ovtcharova M, von Quadt A, Raicheva
988 R (2005) Hydrothermal ore deposits related to post-orogenic extensional magmatism
989 and core complex formation: The Rhodope Massif of Bulgaria and Greece. Ore Geol
990 Rev 27: 53-89
991
992 Márton I, Moritz R, Spikings R (2010) Application of low-temperature
993 thermochronology to hydrothermal ore deposits: formation, preservation and
994 exhumation of epithermal gold system from the Eastern Rhodopes, Bulgaria.
995 Tectonophysics 483: 240–254
996
997 Middlemost EAK (1994) Naming materials in the magma/igneous rock system.
998 Earth- Sci Rev 37: 215–224

Moritz R, Márton I, Ortelli M, Marchev P, Voudouris P, Bonev N, Spikings R, Cosca M (2010) A review of age constraints of epithermal precious and base metal deposits of the Tertiary Eastern Rhodopes: coincidence with Late Eocene–Early Oligocene tectonic plate reorganization along the Tethys. In Christofides G, Kantiradis N, Kostopoulos DS, Chatziperos AA (eds) Proceedings of the XIX Congress of the Carpathian Balkan Geological Association. Scientific Annals of the School of Geology, Thessaloniki, Greece: 351–358

Moritz R, Noverraz C, Marton I, Marchev P, Spikings RA, Fontignie DA, Spangenberg JE, Vennemann T, Kolev K, Hasson S (2014) Sedimentary-rock-hosted epithermal systems of the Tertiary Eastern Rhodopes, Bulgaria: new constraints from the Stremtsi gold prospect. In Garofalo PS, Ridley JS (eds) Gold-transporting hydrothermal fluids in the Earth's crust, Geol Soc London Spec Pub 402: 207-230

Moritz R, Rezeau H, Ovtcharova M, Tayan R, Melkonyan R, Hovakimyan S, Ramazanov V, Selby D, Ulianov A, Chiaradia M, Putlitz B (2016) Long-lived, stationary magmatism and pulsed porphyry systems during Tethyan subduction to post-collision evolution in the southernmost Lesser Caucasus, Armenia and Nakhitchevan. Gondwana Res 37: 465-503

Müller D, Groves DI (2016) Potassic igneous rocks and associated gold-copper mineralization. Springer 4th ed, 311 p

1024 Mutlu AK, Karabulut H (2011) Anisotropic Pn tomography of Turkey and adjacent
1025 regions. Geophys J Int 187: 1743–1758
1026
1027 Mutlu H, Sariz K, Kadir S (2005) Geochemistry and origin of the Şaphane alunite
1028 deposit, Western Anatolia, Turkey. Ore Geol Rev 26: 39–50
1029
1030 Okay A (2008) Geology of Turkey : A synopsis. Anschnitt 21: 19–42
1031
1032 Okay A, Tüysüz O (1999) Tethyan sutures of northern Turkey. In Durand B, Jolivet L,
1033 Horvath F, Seranne M (eds) The Mediterranean basin: Tertiary extension within the
1034 Alpine orogen. Geol Soc London Spec Pub 156: 475–515
1035
1036 Okay A, Satir M, Maluski H, Siyako M, Monie P, Metzger R, Akyüz S (1996) Paleo-
1037 and Neo-Tethyan events in northwestern Turkey: Geologic and geochronologic
1038 constraints. In Yin A, Harrison TM (eds) The tectonic evolution of Asia. Cambridge
1039 University press: 420–441
1040
1041 Okay A, Harris NBW, Kelley SP (1998) Exhumation of blueschists along a Tethyan
1042 suture in northwest Turkey. Tectonophysics 285: 275–299
1043
1044 Oygür V (1997) Anatomy of an epithermal mineralization: Mumcu (Balıkesir-Sındırgı),
1045 inner-western Anatolia, Turkey. Miner Res Expl Bull 119: 29–39
1046
1047 Oygür V, Erler A (2000) Metallogeney of Simav graben (Inner-Western Anatolia,
1048 Turkey). Geol Bull Turkey 43: 7–19

1049

1050 Oyman T, Özgenç I, Tokcaer M, Akbulut M (2013) Petrology, geochemistry, and
1051 evolution of the iron skarns along the northern contact of the Eğrigöz plutonic
1052 complex, western Anatolia, Turkey. Turk J Earth Sci 22: 61–97

1053

1054 Öner Z, Dilek Y (2011) Supradetachment basin evolution during continental
1055 extension: The Aegean province of western Anatolia, Turkey. Geol Soc Am Bull 123:
1056 2115-2141

1057

1058 Patchett PJ, Vervoort JD, Söderlund U, Salters VJM (2004) Lu-Hf and Sm-Nd
1059 isotopic systematics in chondrites and their constraints on the Lu-Hf properties of the
1060 Earth. Earth Planet Sci Lett 222: 29–41

1061

1062 Patiño Douce AE (1999) What do experiments tell us about the relative contributions
1063 of crust and mantle to the origin of granitic magmas? In Castro A, Fernandez C,
1064 Vigneresse JL (eds), Understanding granites: Integrating new and classical
1065 techniques. Geol Soc London Spec Pub 168: 55–75

1066

1067 Pe-Piper G, Piper DJW (2001) Late Cenozoic, post-collisional Aegean igneous rocks:
1068 Nd, Pb and Sr isotopic constraints on petrogenetic and tectonic models. Geol Mag
1069 138: 653–668

1070

1071 Pe-Piper G, Piper DJW (2007) Neogene backarc volcanism of the Aegean: New
1072 insights into the relationship between magmatism and tectonics. In Beccaluva L,
1073 Bianchini G, Wison M (eds) Cenozoic volcanism of the Aegean: New insights into the

relationship between magmatism and tectonics. Geol Soc Am Spec Paper 418: 17–31

Pearce JA (1983) Role of the sub-continental lithosphere in magma genesis at active continental margins. In Hawkesworth CJ, Norry MJ (eds) Continental basalts and mantle xenoliths. Shiva Publishing LTd, Cambridge, Mass: 230-249

Pearce JA, Peate DW (1995) Tectonic implications of the composition of volcanic arc magmas. Annu Rev Earth Planet Sc 23: 251–285

Peccerillo A, Taylor SR (1976) Geochemistry of Eocene calc-alkaline volcanic rocks from the Kastamonu area, northern Turkey. Contrib Mineral Petr 58: 63–81

Perello J, Cox D, Garamjav D, Sanjdorj S, Diakov S, Schissel D, Munkhbat TO, Oyun G (2001) Oyu Tolgoi, Mongolia: Siluro-Devonian porphyry Cu-Au(Mo) and high-sulfidation Cu Mineralization with a Cretaceous chalcocite blanket. Econ Geol 96: 1407–1428

Pettke T, Oberli F, Heinrich CA (2010) The magma and metal source of giant porphyry-type ore deposits, based on lead isotope microanalysis of individual fluid inclusions. Earth Planet Sci Lett 296: 267–277

Plank T (2005) Constraints from Thorium/Lanthanum on sediment recycling at subduction zones and the evolution of the continents. J Petrol 46: 921–944

1099 Plank T, Langmuir C (1993) Tracing trace elements from sediment input to volcanic
1100 output at subduction zones. Nature 362: 739–742
1101
1102 Plank T, Langmuir C (1998) The chemical composition of subducting sediment and
1103 its consequences for the crust and mantle. Chem Geol 145: 325–394
1104
1105 Pourteau A, Candan O, Oberhänsli R (2010) High-pressure metasediments in central
1106 Turkey: Constraints on the Neotethyan closure history. Tectonics 29: TC5004
1107
1108 Rabayrol F, Miskovic A, Hart CJR, Kuşçu İ, Sanchez M (2014) The Cenozoic
1109 metallogeny of Western Anatolia, Turkey. SEG 2014 Meeting: Building Exploration
1110 Capability for the 21st Century, Keystone, Colorado, USA, September 27-30 2016.
1111 http://www.segweb.org/SEG/_Events/Conference_Website_Archives/2014/Conferen
1112 ce_Proceedings/data/index.htm, poster 0393-000197
1113
1114 Rapp RP, Watson, EB, Miller, CF (1991) Partial melting of amphibolite/eclogite and
1115 the origin of Archean trondhjemites and tonalites. Precambrian Res 51: 1–25
1116
1117 Rezeau H, Moritz R, Wotzlaw JF, Tayan R, Melkonyan R, Ulianov A, Selby D,
1118 d'Abzaz FX, Stern R (2016) Temporal and genetic link between incremental pluton
1119 assembly and pulsed porphyry Cu-Mo formation in accretionary orogens. Geology
1120 44: 627-630
1121
1122 Ribeiro JM, Stern RJ, Kelley KA, Martinez F, Ishizuka O, Manton WI, Ohara Y (2013)
1123 Nature and distribution of slab-derived fluids and mantle sources beneath the

1124 southeast Mariana forearc rift. Geochem Geoph Geos 14: 4585–4607
1125
1126 Richards JP (2009) Postsubduction porphyry Cu-Au and epithermal Au deposits:
1127 Products of remelting of subduction-modified lithosphere. Geology 37: 247–250
1128
1129 Richards JP (2011) Magmatic to hydrothermal metal fluxes in convergent and
1130 collided margins. Ore Geol Rev 40: 1–26
1131
1132 Richards JP, Mumin AH (2013) Magmatic-hydrothermal processes within an
1133 evolving Earth: Iron oxide-copper-gold and porphyry Cu±Mo± Au deposits. Geology
1134 41: 767–770
1135
1136 Ring U, Collins AS (2005) U-Pb SIMS dating of synkinematic granites: timing of core-
1137 complex formation in the northern Anatolide belt of western Turkey. J Geol Soc
1138 London 162: 289–298
1139
1140 Ring U, Gessner K, Güngör T, Passchier CW (1999) The Menderes massif of
1141 western Turkey and the Cycladic massif in the Aegean—do they really correlate? J
1142 Geol Soc London 156: 3–6
1143
1144 Ring U, Johnson C, Hetzel R, Gessner K (2003) Tectonic denudation of a Late
1145 Cretaceous-Tertiary collisional belt: regionally symmetric cooling patterns and their
1146 relation to extensional faults in the Anatolide belt of western Turkey. Geol Mag 140:
1147 421–441
1148

1149 Ring U, Glodny J, Will T, Thomson S (2010) The Hellenic subduction system: High-
1150 pressure metamorphism, exhumation, normal faulting, and large-scale extension.
1151 Annu Rev Earth Planet Sc 38: 45–76
1152
1153 Roberts MP, Clemens JD (1993) Origin of high-potassium, calc-alkaline, I-type
1154 granitoids. Geology 21: 825–828
1155
1156 Rudnick RL, Gao S (2003) Composition of the continental crust. In Rudnick RL,
1157 Holland HD, Turekian KK (eds), The crust, Treatise on Geochemistry, Elsevier: 1–64
1158
1159 Sánchez MG, McClay KR, King AR, Wijbrams JR (2016) Cenozoic crustal extension
1160 and its relationship to porphyry Cu-Au-(Mo) and epithermal Au-(Ag) mineralization in
1161 the Biga Peninsula, northwestern Turkey. In: Richards JP (ed), Tectonics and
1162 metallogeny of the Tethyan orogenic belt, Soc Econ Geol Spec Pub 19: 113–156
1163
1164 Selby D, Creaser RA (2001) Late and mid-Cretaceous mineralization in the northern
1165 Canadian Cordillera: Constraints from Re-Os molybdenite dates. Econ Geol 96:
1166 1461–1467
1167
1168 Seyitoglu G (1997) The Simav Graben: An example of young E-W trending structures
1169 in the Late Cenozoic extensional system of W. Turkey. Turk J Earth Sci 6: 135–141
1170
1171 Seyitoglu G, Scott BC, Rundle CC (1992) Timing of Cenozoic extensional tectonics in
1172 west Turkey. J Geol Soc London 149: 533–538
1173

1174 Sherlock SC (1999) Oscillatory zoned chrome lawsonite in the Tavşanlı zone,
1175 northwest Turkey. Mineral Mag 63: 687–692
1176
1177 Sillitoe RH (2002) Some metallogenic features of gold and copper deposits related to
1178 alkaline rocks and consequences for exploration. Mineral Deposita 37: 4–13
1179
1180 Smoliar MI, Walker RJ, Morgan JW (1996) Re-Os ages of group IIA, IIIA, IVA, and
1181 IVB iron meteorites. Science 271: 1099–1102
1182 Spakman W, Wortel MJR, Vlaar NJ (1988) The Hellenic subduction zone: A
1183 tomographic image and its geodynamic implications. Geophys Res Lett 15: 60–63
1184
1185 Sun SS, McDonough WF (1989) Chemical and isotopic systematics of oceanic
1186 basalts: implications for mantle composition and processes. In Saunders AD, Norry
1187 MJ (eds) Magmatism in the ocean basins. Geol Soc London Spec Pub 42: 313–345
1188
1189 Şengör AMC, Yilmaz Y (1981) Tethyan evolution of Turkey: A plate tectonic
1190 approach. Tectonophysics 75: 181–241
1191
1192 Şengör AMC, Satir M, Akkök R (1984) Timing of tectonic events in the Menderes
1193 massif, western Turkey: Implications for tectonic evolution and evidence for pan-
1194 African basement in Turkey. Tectonics 3: 693–707
1195
1196 Tatsumi Y, Hamilton DL, Nesbitt RW (1986) Chemical characteristics of fluid phase
1197 released from a subducted lithosphere and origin of arc magmas: Evidence from
1198 high-pressure experiments and natural rocks. J Volcanol Geoth Res 29: 293–309

Thirwall M, Smith TE, Graham AM, Theodorou N, Hollings P. Davidson JP, Arculus RD (1994) High field strength element anomalies in arc lavas: source or processes. J Petrol 35: 819–838

Thorpe RS, Francis PW (1979) Variations in Andean andesite compositions and their petrogenetic significance. Tectonophysics 57: 53–70

Tokay M, Doyuran V (1979) Seismotectonic features of Gediz and its surroundings. Geol Bull Turkey 22: 209–210 (in Turkish with English abstract)

van Hinsbergen DJJ (2010) A key extensional metamorphic complex reviewed and restored: The Menderes massif of western Turkey. Earth-Sci Rev 102: 60–76

van Hinsbergen DJJ, Schmid SM (2012) Map view restoration of Aegean–West Anatolian accretion and extension since the Eocene. Tectonics 31: TC5005

Vigneresse JL (2007) The role of discontinuous magma inputs in felsic magma and ore generation. Ore Geol Rev 30: 181–216

Voudouris P, Melfos V, Moritz R, Spry PG, Ortelli M, Kartal, T (2010) Molybdenite occurrences in Greece: Mineralogy, geochemistry and rhenium content. In Christofides G, Kantiradis N, Kostopoulos DS, Chatziperos AA (eds) Proceedings of the XIX Congress of the Carpathian Balkan Geological Association. Scientific Annals of the School of Geology, Thessaloniki, Greece: 369–378

Voudouris P, Melfos V, Spry PG, Kartal T, Schleicher H, Moritz R, Ortelli M (2013a) The Pagoni Rachi/Kirki Cu-Mo±Re±Au deposit, northern Greece: Mineralogical and fluid inclusion constrains on the evolution of a telescoped porphyry-epithermal system. Can Mineral 51: 411–442

Voudouris P, Melfos V, Spry PG, Bindi L, Moritz R, Ortelli M, Kartal T (2013b) Extremely Re-rich molybdenite from porphyry Cu-Mo-Au prospects in northeastern Greece: Mode of occurrence, causes of enrichment, and implications for gold exploration. Minerals 3: 165–191

Wasserburg G, Jacousen S, DePaolo D, McCulloch M, Wen T (1981) Precise determination of Sm/Nd ratios, Sm and Nd isotopic abundances in standard solutions. Geochim Cosmochim Acta 45: 2311–2323

Whitney DL, Bozkurt E (2002) Metamorphic history of the southern Menderes massif, western Turkey. Bull Geol Soc Am 114: 829–838

Winchester JA, Floyd PA (1977) Geochemical discrimination of different magma series and their differentiation products using immobile elements. Chem Geol 20: 325–343

Yiğit Ö (2006) Gold in Turkey — a missing link in Tethyan metallogeny. Ore Geol Rev 28: 147–179

1249 Yiğit Ö (2009) Mineral deposits of Turkey in relation to Tethyan metallogeny:
1250 implications for future mineral exploration. Econ Geol 104: 19–51
1251
1252 Yilmaz Y (1989) An approach to the origin of young volcanic rocks of western Turkey.
1253 In: Şengör AMC (ed), Tectonic evolution of the Tethyan region. SE - 10, NATO ASI
1254 Series. Springer: 159–189
1255
1256 Zartman RE, Doe BR (1981) Plumbotectonics — the model. Tectonophysics 75:
1257 135–162
1258
1259 Zhao JH, Zhou MF (2007) Geochemistry of Neoproterozoic mafic intrusions in the
1260 Panzhihua district (Sichuan Province, SW China): Implications for subduction-related
1261 metasomatism in the upper mantle. Precambrian Res 152: 27-47
1262
1263 Zindler A, Hart S (1986) Chemical Geodynamics. Annu Rev. Earth Planet Sci 14:
1264 493–571
1265
1266
1267

Figure Captions

Fig. 1 Simplified regional tectonic-geological map of western Anatolia and location of the Pınarbaşı Mo-Cu prospect and major ore deposits/prospects related with the main tectonic structures in western Anatolia (modified after Dilek et al. 2009; Öner and Dilek 2011). Inset shows main plate boundaries, major suture zones, metamorphic massifs and tectonic units of the Aegean and eastern Mediterranean region (modified after Dilek 2006; Dilek and Sandvol 2009; Okay and Tüysüz 1999) BFZ: Bornava flysch zone; CACC: Central Anatolian Crystalline Complex; EAFZ: East Anatolian fault zone; EF: Ecemis fault; KA: Kazdağ massif; IASZ: Izmir–Ankara suture zone; ITSZ: Inner–Tauride suture zone; MM: Menderes massif; NAFZ: North Anatolian fault zone.

Fig. 2 a Simplified geological map of the Pınarbaşı (Gediz) prospect (Delibaş et al. 2012a, b), inset shows location of the Pınarbaşı Mo-Cu prospect within the Erdoğmuş-Yenigediz graben (modified after Gürboğa et al. 2013), **b** generalized stratigraphic column of the study area (modified after Akdeniz and Konak 1979; Delibaş et al. 2012a, b)

Fig. 3 Field relationships at the Pınarbaşı prospect. **a** EW-trending normal fault system cutting monzonite and associated silicified zones, **b** NE-trending late stage normal fault cutting supergene argillic alteration zones, **c** contact relationships between monzonite and limestone, **d** magnetite-epidote-pyroxene skarn zones along contacts of a NW-trending porphyritic granite dyke with ultramafic rocks of the ophiolitic mélange unit, **e** drill core sample showing porphyritic granite crosscutting

monzonite, **f** intrusion breccia formed during emplacement of porphyritic granite into monzonite

Fig. 4 Different mineralization types at the Pınarbaşı prospect. **a** Pyrite-molybdenite and chalcopyrite-bearing stockwork quartz-limonite veins crosscutting monzonite with intense sericitic alteration and stockwork-type mineralization crosscut by late stage strike-slip and normal fault systems, **b** NE and EW-striking quartz-molybdenite±chalcopyrite veins crosscutting porphyritic granite, **c** drill core sample with quartz-molybdenite vein surrounded by sericitic alteration, **d** molybdenite-bearing intensely silicified zone, **e** drill core sample consisting of a quartz-molybdenite-pyrite-chalcopyrite vein (Qz: quartz, Py: pyrite, Ccp: chalcopyrite, Mol: molybdenite, Lm: limonite)

Fig. 5 Alteration styles and alteration minerals from the Pınarbaşı prospect. **a** Magnetite veins crosscutting porphyritic granite, **b** K-feldspar vein crosscutting porphyritic granite, **c** biotite replaced by sericite around quartz-molybdenite veins, **d** muscovite within sericitic alteration zones, **e** fibroradial pyrophyllite crystals within the advanced argillic alteration zone, **f** tabular alunite crystals within the advanced argillic alteration zone (Qz: quartz, Bt: biotite, Ser: sericite, Ms: muscovite, Prl: pyrophyllite, Alu: alunite)

Fig. 6 Geochemical classification and discrimination diagrams including magmatic rock samples from the Pınarbaşı prospect. **a** SiO_2 (wt.%) versus Na_2O+K_2O (wt.%) classification diagram (Middlemost 1994), **b** AFM plot of Irvine and Baragar (1971), A: Na_2O+K_2O (wt.%); F: FeO_t (wt.%); M: MgO (wt.%), **c** K_2O (wt.%) versus SiO_2

(wt.%) diagram for the samples of Pınarbaşı granitoid (discrimination lines separating the tholeiitic, calc-alkaline, high-K calc-alkaline and shoshonitic series are from Peccerillo and Taylor 1976), **d** Al/(Ca+Na+K) versus Al/(Na+K) molar discrimination diagram (OMG: Oligo-Miocene Granitoids; Altunkaynak et al. 2012a)

Fig. 7 a Primitive mantle-normalized (Sun and McDonough 1989) multi-element patterns for rock samples from the Pınarbaşı pluton, **b** chondrite-normalized (Sun and McDonough 1989) REE patterns for rock samples from the Pınarbaşı pluton (Upper and Lower Crust data from Rudnick and Gao 2003; data for Menderes Massif metamorphic rocks from Çoban et al. 2012)

Fig. 8 Pb, Nd and Sr isotopic compositions of rock samples from the Pınarbaşı pluton compared with various potential source reservoirs and rocks. The composition of present-day CHUR was calculated for 20 Ma. Lead isotope Upper Crust and Orogen curves from Zartman and Doe (1981). BG: Baklan Granitoid (Aydoğan et al. 2008); BSE: Bulk silicate earth from Zindler and Hart (1986); DMM: Depleted MORB; EM1: Enriched mantle I; EM2: Enriched mantle II; EMSS: Eastern Mediterranean Sea Sediments (Klaver et al. 2015); EOG: Eocene Granitoids (Altunkaynak et al. 2012b); GLOSS: Global Subducted Sediments (Plank and Langmuir 1998); KV: Kula volcanic rocks (Güleç 1991; Alici et al. 2002; Innocenti et al. 2005; Dilek and Altunkaynak 2010; Chakrabarti et al. 2012); MMM: Menderes Massif metamorphic rocks (Çoban et al. 2012); OMG: Oligo-Miocene Granitoids (Altunkaynak et al. 2012a); SMV: Simav volcanic-subvolcanic rocks (Çoban et al. 2012)

Fig. 9 Trace element and isotope variation diagrams for magmatic rocks from the Pınarbaşı pluton: **a** Dy/Yb versus SiO2 (wt.%), **b** Zr/Sm versus SiO2 (wt.%) ,**c** initial $^{87}Sr/^{86}Sr$ versus 1/Sr (1/ppm), **d** SiO_2 (wt.%) versus initial $^{208}Pb/^{204}Pb$ isotope ratios (AFC: assimilation + fractional crystallization trend from DePaolo 1981)

Fig. 10 **a** ($Na_2O+K_2O+Fe_2O_3+MgO+TiO_2$) versus $Na_2O+K_2O)/(Fe_2O_3+MgO+TiO_2$) discrimination plot for granite melt sources (Patiño Douce 1999), **b** La (ppm) versus La/Yb diagram, with partial melting and fractional crystallization trends from Thirlwall et al. (1994), **c** La/Sm versus Sm/Yb diagram, with pressure-dependent pyroxene and amphibole stabilities from Kay and Mpodozis (2001), **d** Nb–Y–Ga*3 granite classification diagram after Eby (1992). BG: Baklan granitoid (Aydoğan et al. 2008); EG: Eğrigöz granitoid (Altunkaynak et al. 2012a, Çoban et al. 2012); SMV: Simav volcanic-subvolcanic rocks (Çoban et al. 2012)

Fig. 11 **a** Ta/Yb versus Th/Yb discrimination diagram after Pearce (1983), **b** Nb/Yb versus Ba (ppm) diagram, **c** Nb/Y versus Rb/Y diagram, fluid- and melt-related enrichment trends from Zhao and Zhou (2007), **d** Ba/Th versus Th/Nb diagram, **e** Ba/La versus Th/Yb diagram, **f** Th/Nb versus Ba/Nb diagram with sediment melt and aqueous fluids trends from Ribeiro et al. (2013). MORB data from Hofmann (1997). BG: Baklan granitoid (Aydoğan et al. 2008); EG: Eğrigöz granitoid (Altunkaynak et al. 2012a, Çoban et al. 2012); EMSS: Eastern Mediterranean Sea Sediments (Klaver et al. 2015); GLOSS: Global Subducted Sediments (Plank and Langmuir 1998)

Fig. 12 Summary of major tectonic and magmatic events within western Anatolia from Oligocene to Miocene. 1: Jolivet and Brun (2010), van Hinsbergen (2010),

Jolivet et al. (2015); 2-3: Spakman et al. (1988), Jolivet and Brun (2010), van Hinsbergen (2010), Erkül et al. (2013), Ersoy and Palmer (2013), Jolivet et al. (2013, 2015); 4: Yilmaz (1989), Bozkurt et al. (1993), Hetzel et al. (1995), Bozkurt and Park (1997), Ring et al. (1999, 2010), Koçyiğit et al. (2000), Whitney and Bozkurt (2002), Bozkurt and Sözbilir (2004), Dilek et al. (2009), Agostini et al. (2010); 5: Isik et al. (2004), Ring and Collins (2005), Aydoğan et al. (2008), Hasözbek et al. (2010), Altunkaynak et al. (2012a); 6: Dilek et al. (2009), Altunkaynak et al. (2012a); 7: Doglioni et al. (2002), Innocentini et al. (2005), Agostini et al. (2007, 2010), Helvacı et al. (2009), Karaoğlu et al. (2010), Ersoy and Palmer (2013)

Figure1

Click here to download Figure figure1 4th rev RM.jpg

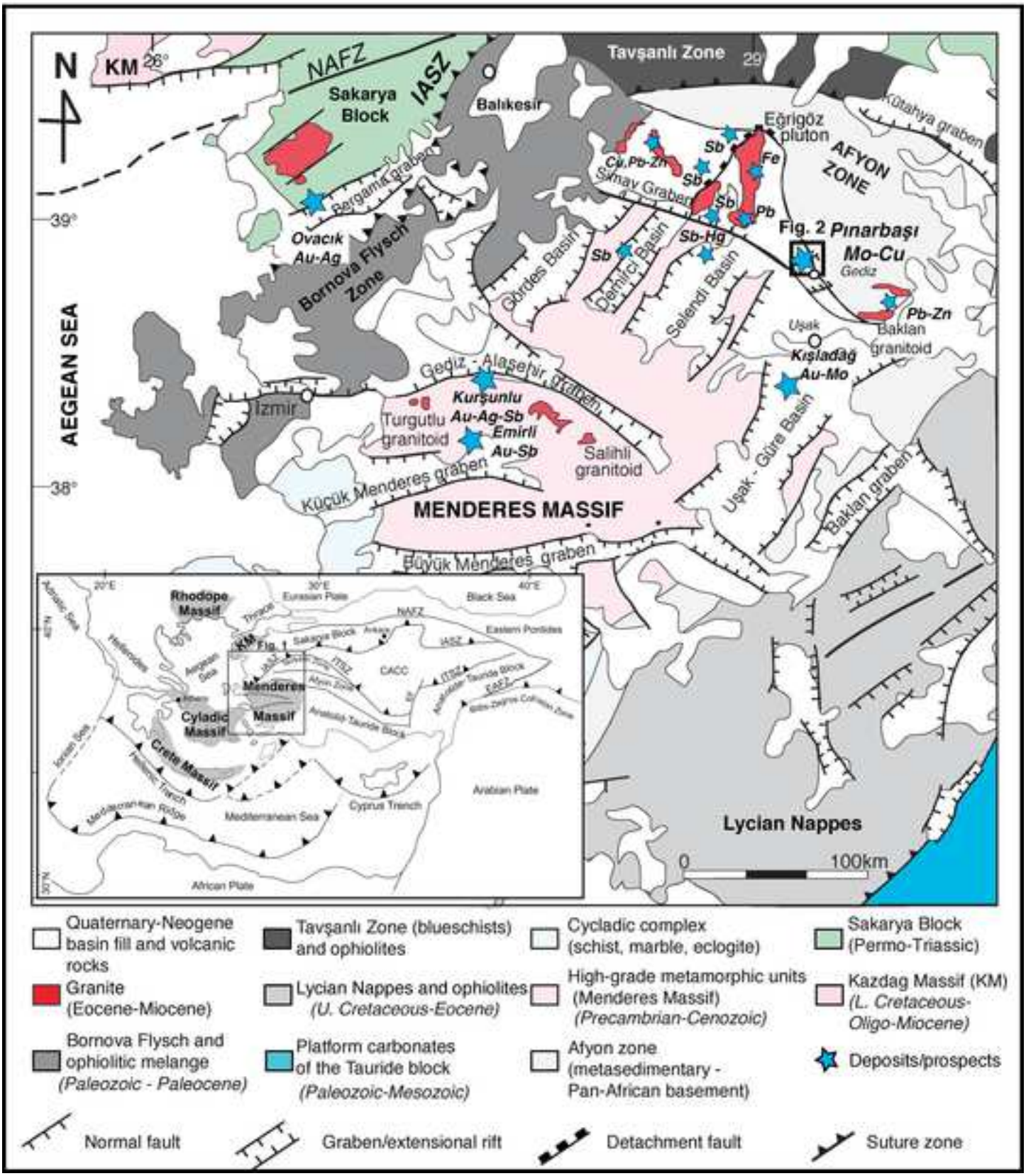

Figure2

Click here to download Figure figure2 4th rev.jpg

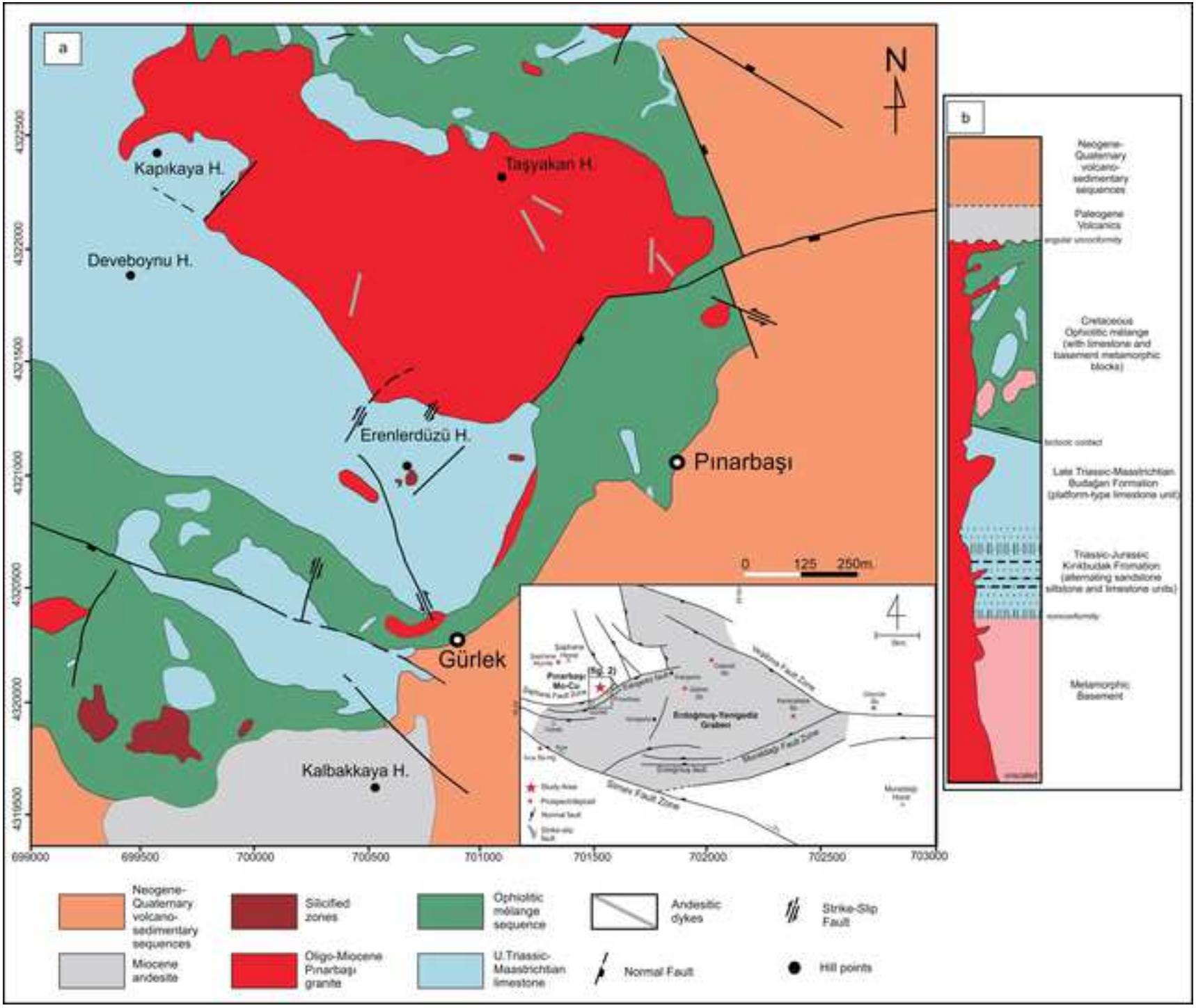

Figure3

Click here to download Figure figure3rev.jpg

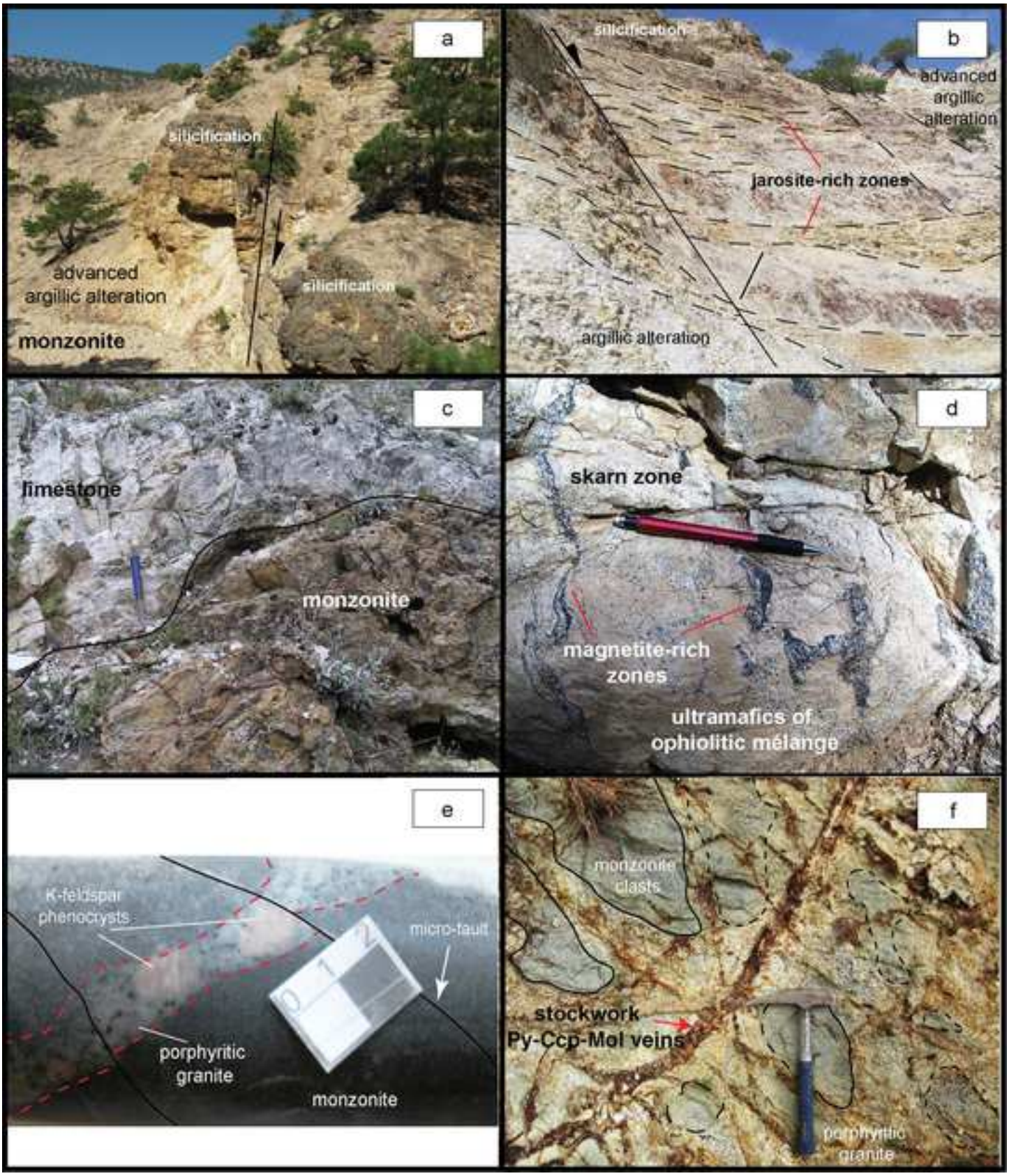

Figure4

Click here to download Figure figure4.jpg

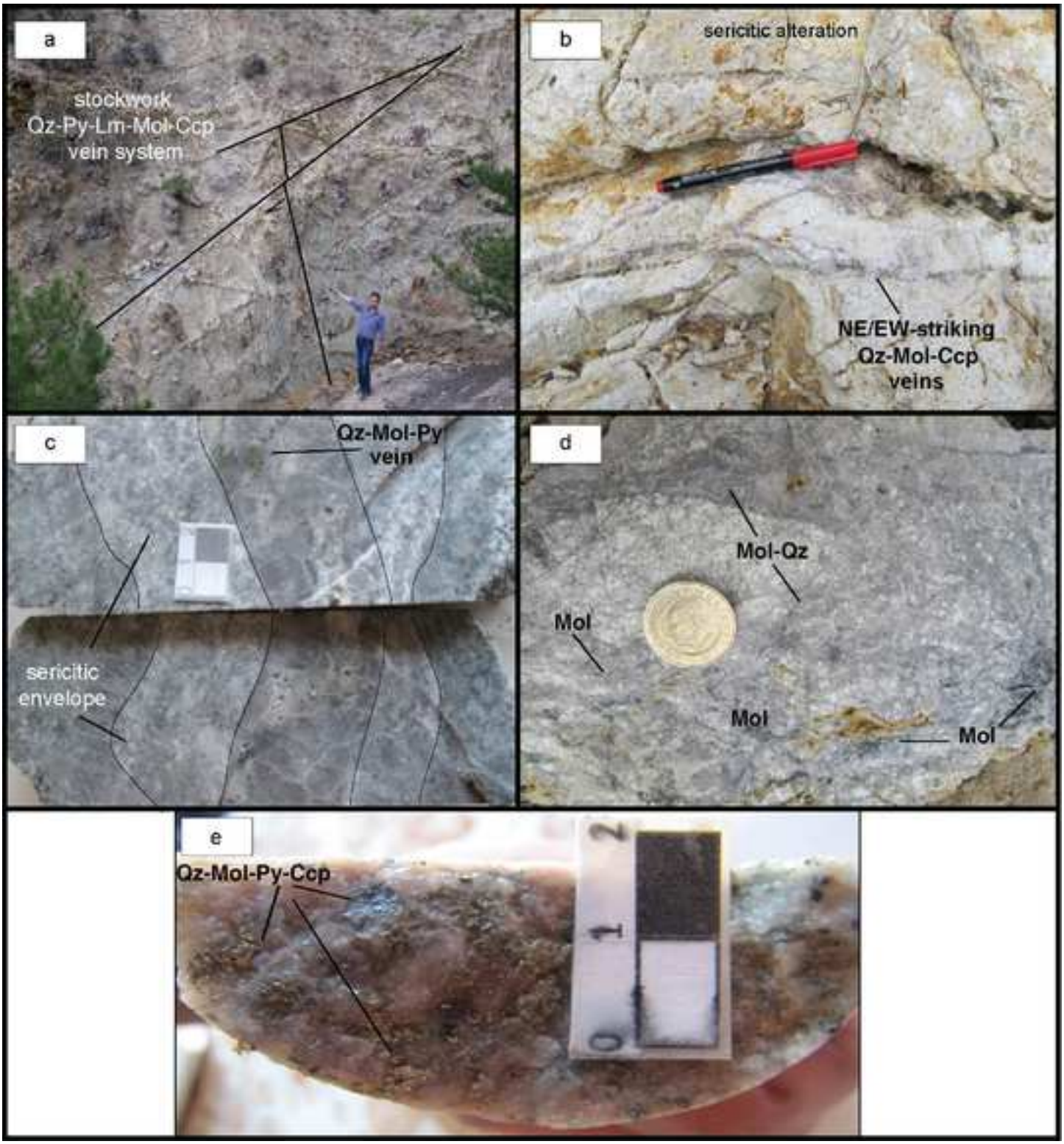

Figure5

Click here to download Figure figure5arev.jpg

Figure6

Click here to download Figure figure6b.jpg

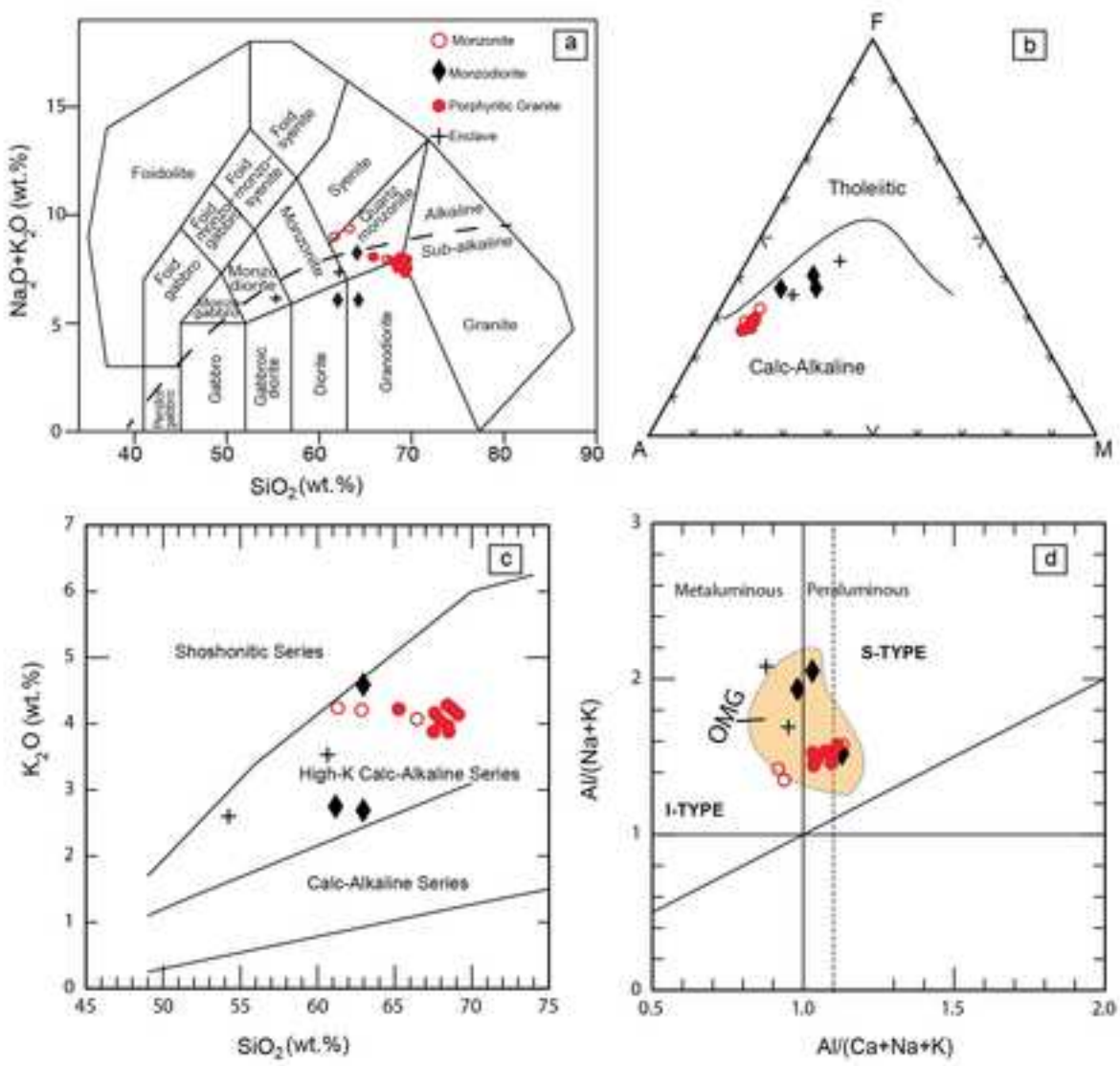

Figure7

Click here to download Figure figure7b.jpg

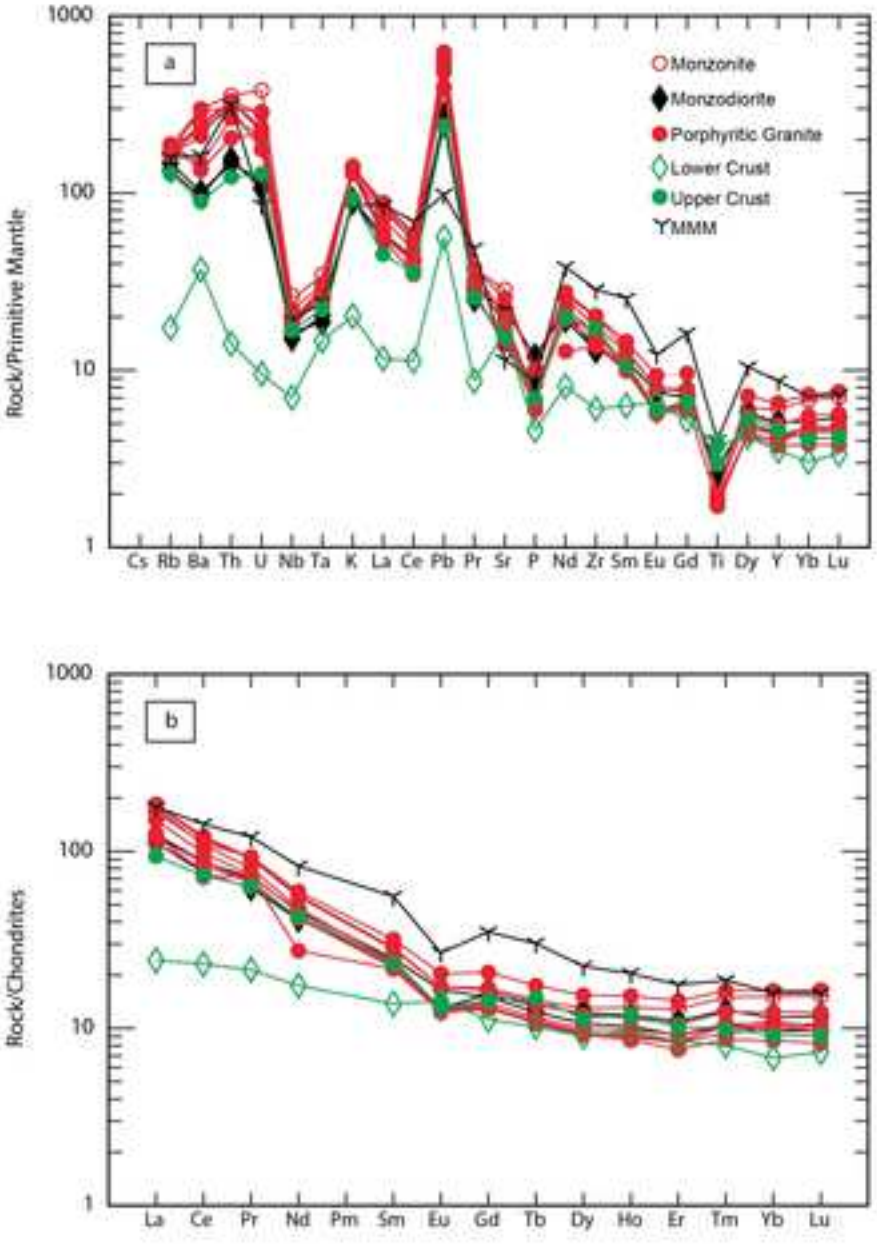

Figure8

Click here to download Figure figure8b.jpg

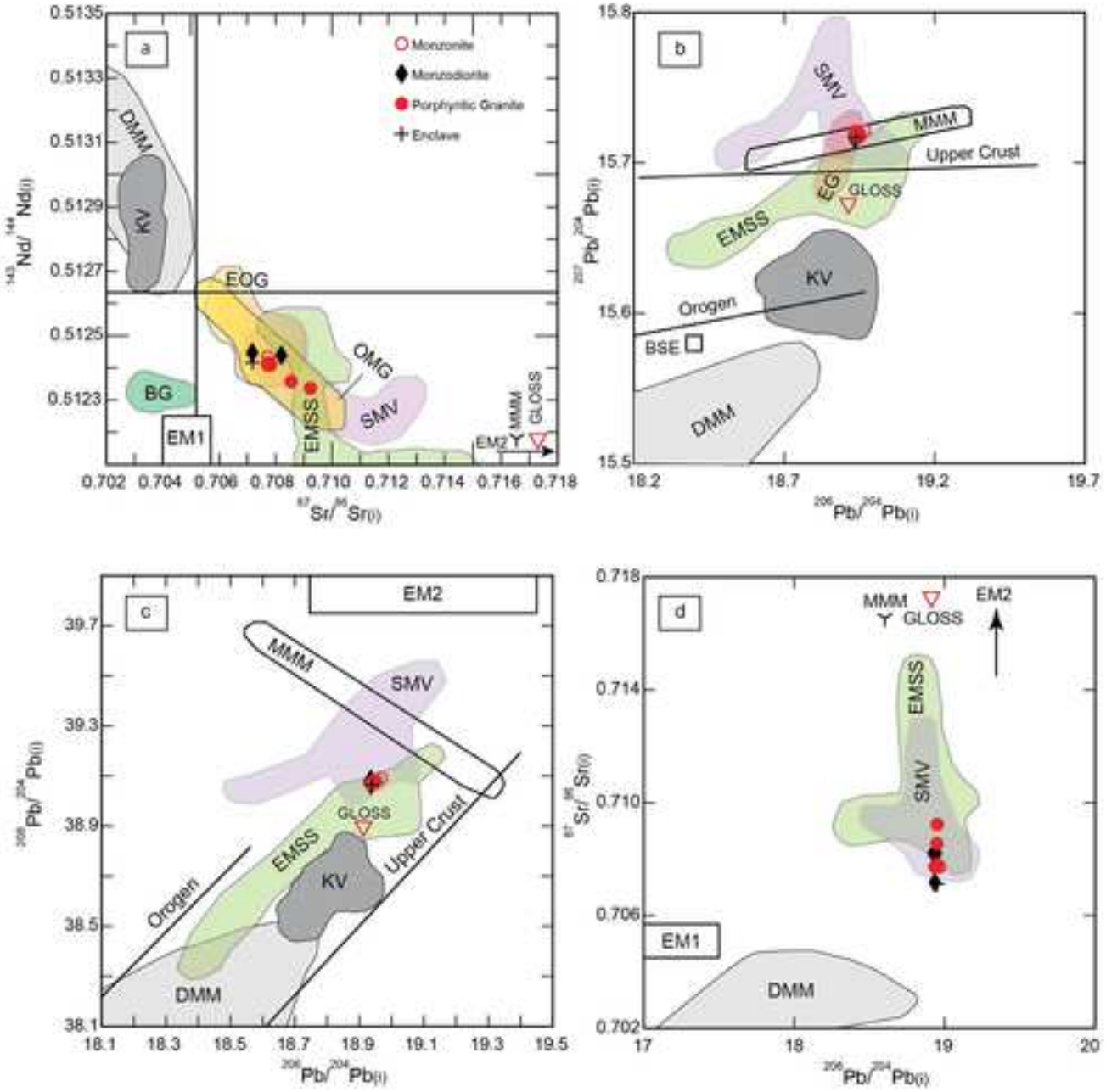

Figure9

Click here to download Figure figure9b.jpg

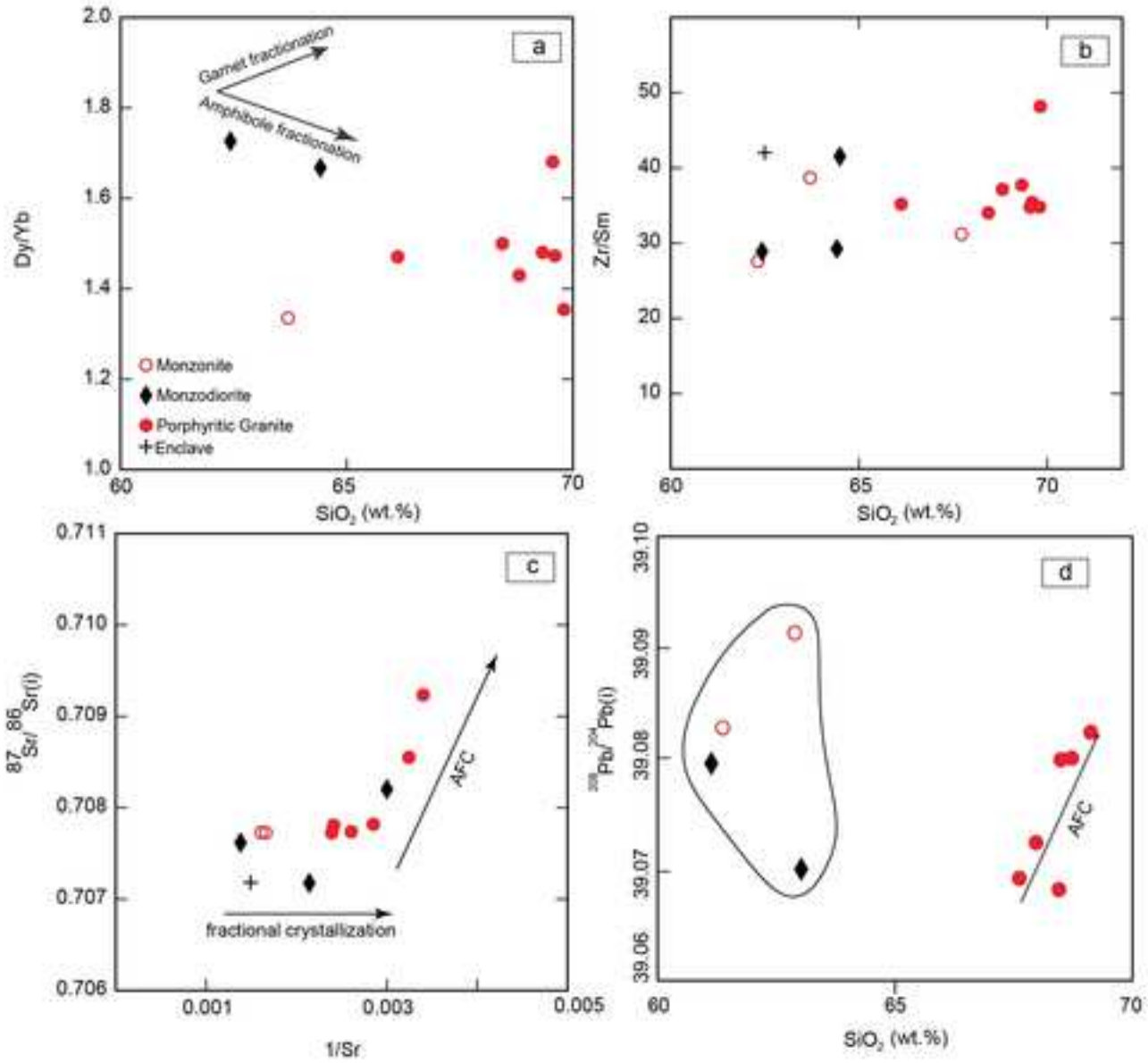

Figure10

Click here to download Figure figure10rev.jpg

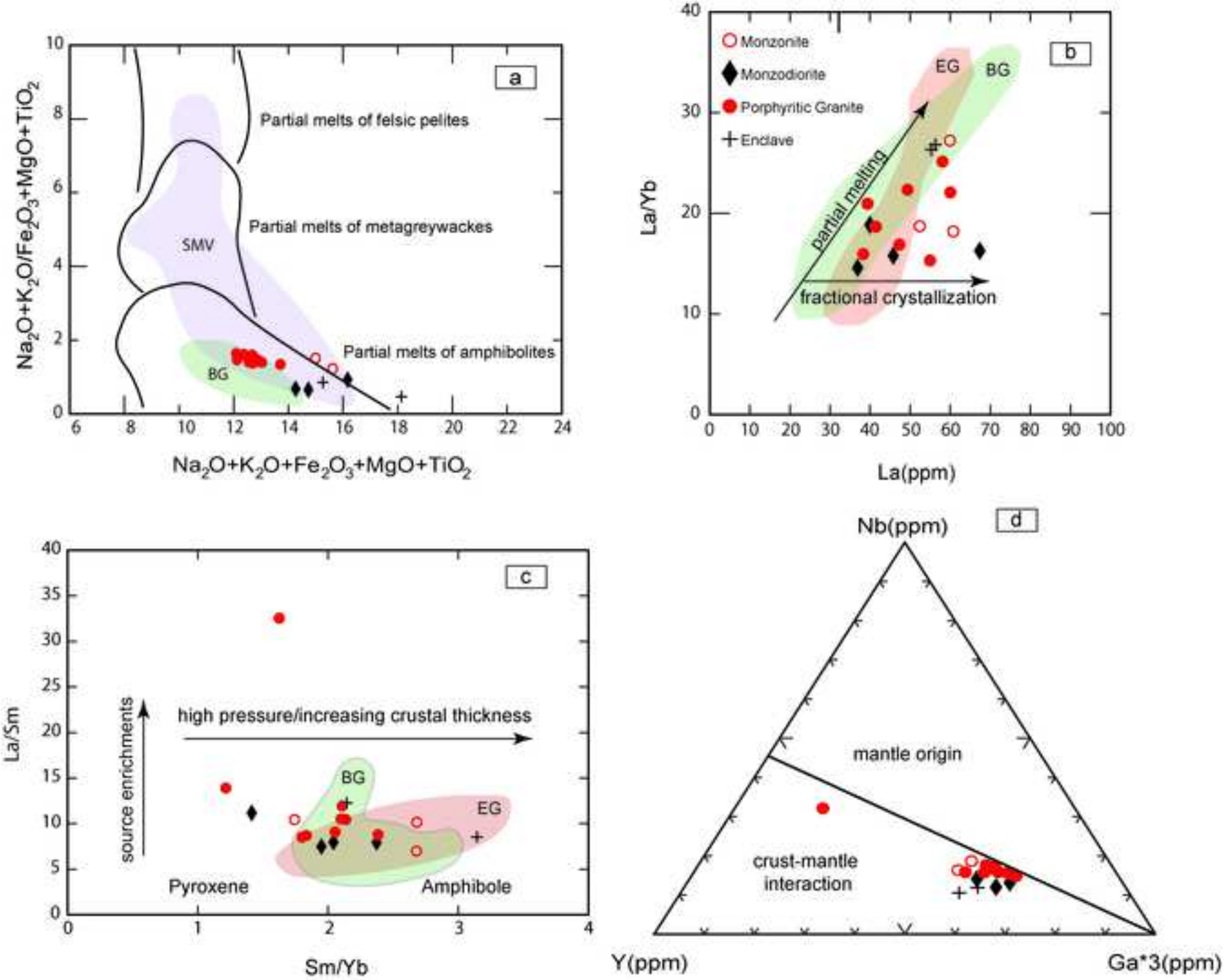

Figure11

Click here to download Figure figure11rev.jpg

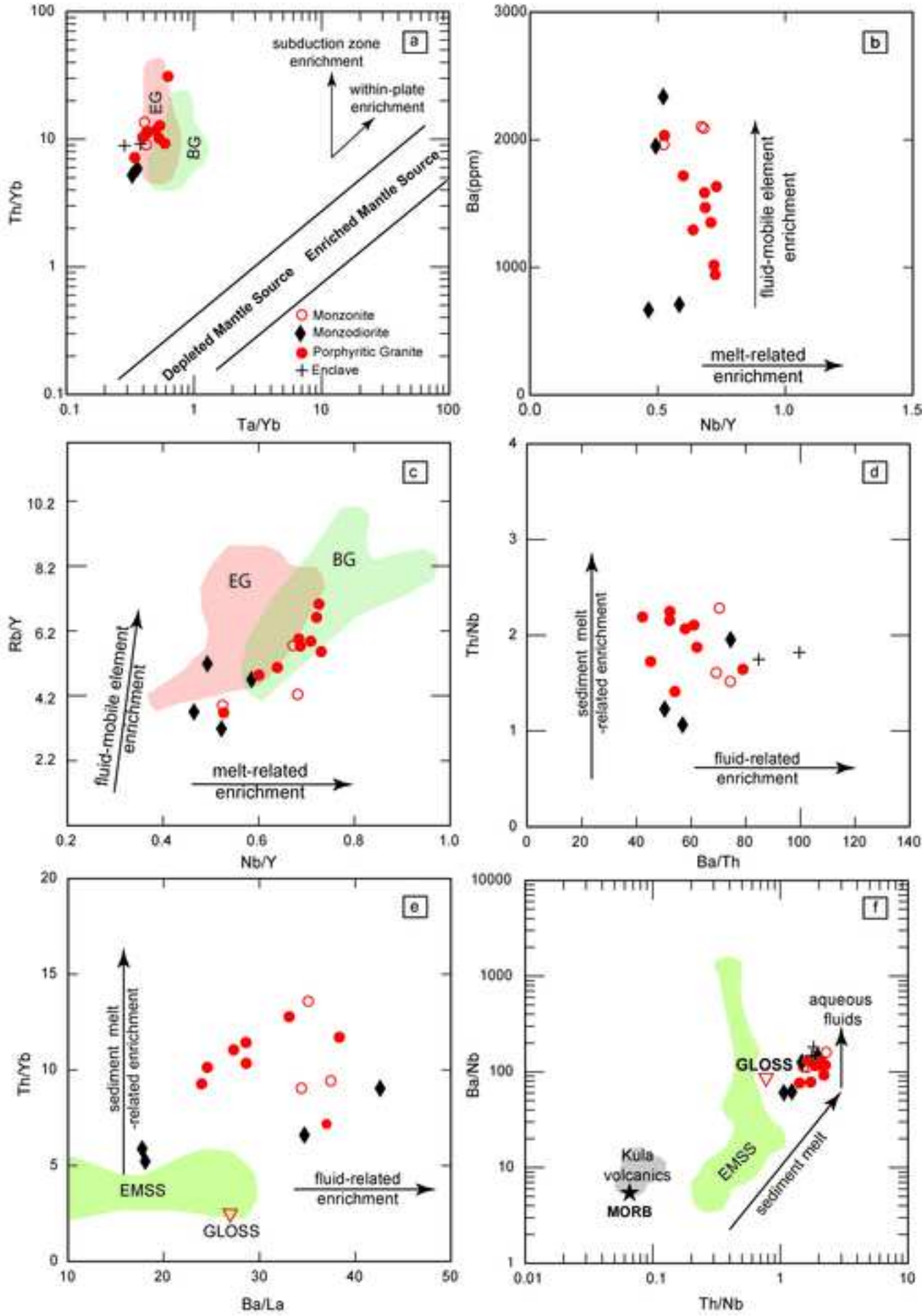

Figure12

Click here to download Figure figure12rev.jpg

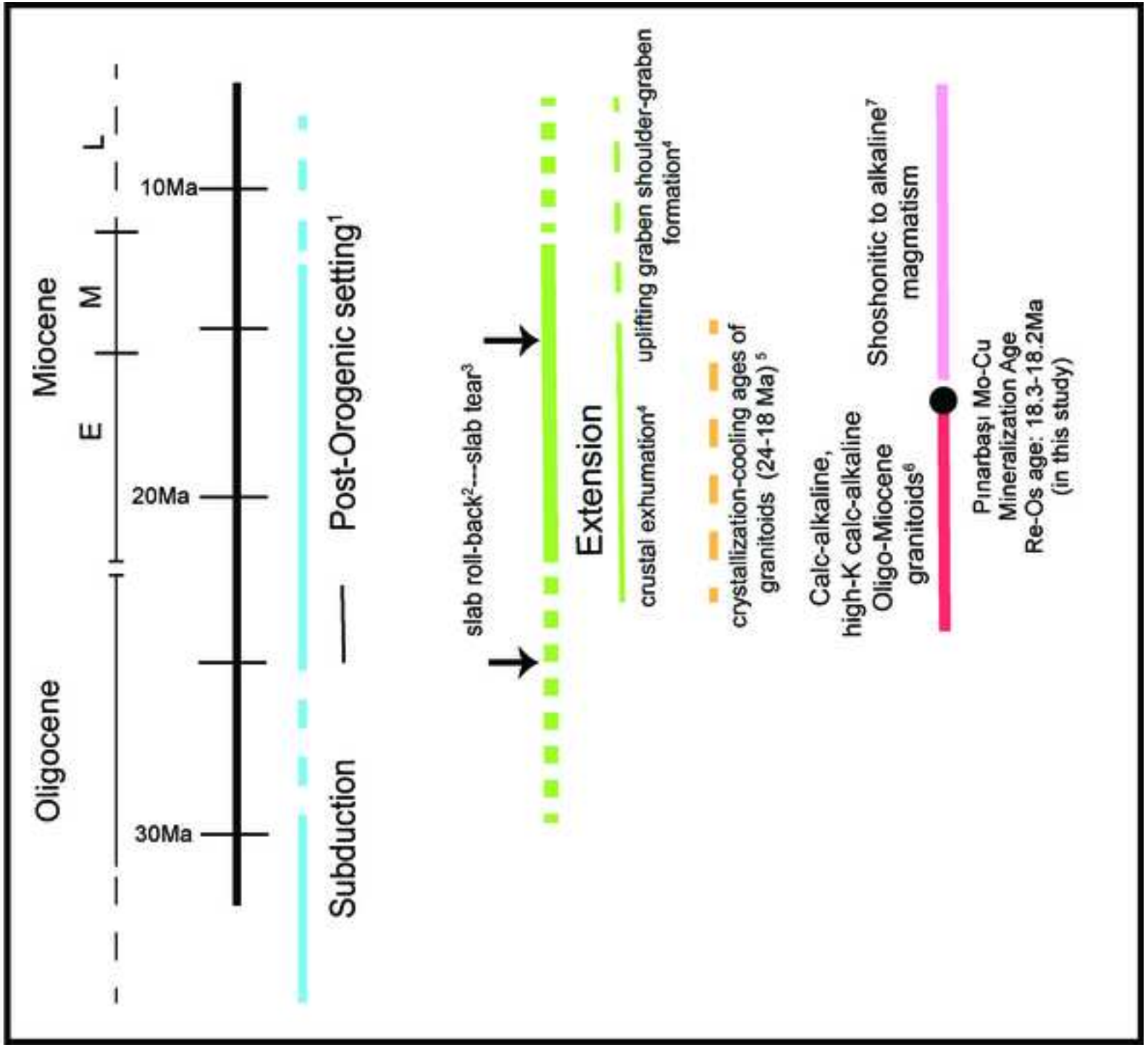

Table1

Table 1 Isotope data (Sr and Nd) of magmatic whole rock samples from the Pınarbaşı intrusion.

Sample No	87Sr/86Sr	Rb (ppm)	Sr (ppm)	87Sr/86Sr(i)	143Nd/144Nd	Sm (ppm)	Nd (ppm)	143Nd/144Nd(i)	enD
GOTK1	0.70790	130	621	**0.70773**	0.51244	7.5	28.9	**0.51241**	**-3.9**
GOTK2	0.70789	117	602	**0.70787**	0.51245	5.8	35.6	**0.51243**	**-3.5**
GOTK9	0.70734	94	467	**0.70718**	0.51246	5.0	29.3	**0.51245**	**-3.2**
GOTK11	0.70799	118	384	**0.70774**	0.51243	4.9	30.3	**0.51242**	**-3.8**
GOTK6	0.70887	120	308	**0.70855**	0.51237	4.6	26.4	**0.51236**	**-5.0**
GOTK12	0.70775	113	724	**0.70762**	0.51230	8.5	47.6	**0.51228**	**-6.5**
GOTK13	0.70801	104	415	**0.70781**	0.51242	4.7	28.4	**0.51241**	**-4.0**
GOTK14	0.70841	86	333	**0.70820**	0.51245	4.9	26.0	**0.51244**	**-3.4**
GOTK15	0.70957	119	294	**0.70923**	0.51235	4.5	26.4	**0.51234**	**-5.4**
GOTK7	0.70805	105	369	**0.70782**	0.51243	4.5	27.5	**0.51241**	**-3.9**
GOTK16	0.70794	108	418	**0.70773**	0.51242	5.7	34.8	**0.51241**	**-4.0**
GOTK3	0.70735	118	591	**0.70718**	0.51245	3.9	27.0	**0.51244**	**-3.4**

Note: enD values are calculated relative to CHUR with present day values of $(^{143}Nd/^{144}Nd)_{chur}$ =0.512638 and $^{147}Sm/^{144}Nd$=0.1967, $\lambda^{147}Sm=6.54\times10^{-12}$ enD: $((^{143}Nd/^{144}Nd)_{sample}/(^{143}Nd/^{144}Nd)_{CHUR}-1))*10.000$ (Wasserburg et al. 1981; Jacobsen and Wasserburg 1984). Initial values are calculated for an assumed age of 20 Ma.

Table 2 Isotope data (Pb) of magmatic whole rock samples from the Pınarbaşı intrusion.

Sample No	206/204Pb	207/204Pb	208/204Pb	Pb ppm	U ppm	Th ppm	206Pb/Pb204(i)	207Pb/204Pb(i)	208Pb/204Pb(i)
GOTK01	18.992	15.719	39.126	40.5	9.2	26.4	**18.946**	**15.717**	**39.083**
GOTK02	19.001	15.723	39.139	41.5	7.0	30.0	**18.967**	**15.721**	**39.091**
GOTK09	18.961	15.719	39.122	19.6	2.5	12.5	**18.935**	**15.718**	**39.080**
GOTK12	19.044	15.725	39.124	49.6	5.7	27.3	**19.021**	**15.724**	**39.088**
GOTK14	18.961	15.717	39.121	17.3	2.2	13.2	**18.935**	**15.716**	**39.070**
GOTK06	18.975	15.721	39.124	34.0	4.4	22.5	**18.949**	**15.720**	**39.080**
GOTK07	18.977	15.721	39.138	34.1	5.0	28.7	**18.948**	**15.720**	**39.082**
GOTK11	18.969	15.718	39.129	27.8	3.7	25.5	**18.942**	**15.717**	**39.068**
GOTK13	18.984	15.721	39.139	28.1	4.9	28.2	**18.949**	**15.719**	**39.073**
GOTK15	18.976	15.719	39.111	37.2	4.6	17.4	**18.951**	**15.718**	**39.080**
GOTK16	18.959	15.722	39.116	39.8	4.6	28.1	**18.936**	**15.721**	**39.069**
GOTK3	18.976	15.719	39.111	43.0	8.0	30.2	**18.939**	**15.717**	**39.065**

Table3

Table 3 Re-Os data for molybdenite from the Pınarbaşı prospect

Sample No	wt (g)	Re (ppm) ± 2σ	^{187}Re (ppm) ± 2σ	^{187}Os (ppb) ± 2σ	Age (Ma) ± 2σ (1)	Age (Ma) ± 2σ (2)
GOP-19m	0.01047	950.3 ± 4.7	597.3 ± 3.0	181.2 ± 0.8	18.21 ± 0.07	18.21 ± 0.09
OKY3-4	0.01014	1035.5 ± 5.2	650.8 ± 3.3	198.5 ± 0.9	18.30 ± 0.07	18.30 ± 0.09

Re-Os dates are calculated using Re decay constants from Smoliar et al. (1996)
(1) age uncertainty includes all sources of analytical uncertainty
(2) age uncertainty includes all sources of analytical uncertainty and that of the decay constant.

Supplementary Material2

Supplementary Material3

Supplementary Material4